CHEMICAL
RESEARCH,
DEVELOPMENT &
ENGINEERING
CENTER

(2)

CRDEC-CR-88068

METHODS AND MEASUREMENTS OF EXTINCTION PROPERTIES OF OBSCURANTS FOR INFRARED TO MILLIMETER WAVE REGION

by K. D. Moeller
V. P. Tomaselli

FAIRLEIGH DICKINSON UNIVERSITY
Teaneck, NJ 07666

May 1988

U.S. ARMY
ARMAMENT
MUNITIONS
CHEMICAL COMMAND

Aberdeen Proving Ground, Maryland 21010-5423

Disclaimer

The findings in this report are not to be construed as an official Department of the Army position unless so designated by other authorizing documents.

Distribution Statement

Approved for public release; distribution is unlimited.

UNCLASSIFIED
SECURITY CLASSIFICATION OF THIS PAGE

REPORT DOCUMENTATION PAGE

Form Approved OMB No. 0704-0188

1a. REPORT SECURITY CLASSIFICATION: UNCLASSIFIED	1b. RESTRICTIVE MARKINGS
2a. SECURITY CLASSIFICATION AUTHORITY	3. DISTRIBUTION/AVAILABILITY OF REPORT: Approved for public release; distribution is unlimited.
2b. DECLASSIFICATION/DOWNGRADING SCHEDULE	
4. PERFORMING ORGANIZATION REPORT NUMBER(S): CRDEC-CR-88068	5. MONITORING ORGANIZATION REPORT NUMBER(S)
6a. NAME OF PERFORMING ORGANIZATION: Fairleigh Dickinson University; 6b. OFFICE SYMBOL (If applicable)	7a. NAME OF MONITORING ORGANIZATION
6c. ADDRESS (City, State, and ZIP Code): Teaneck, NJ 07666	7b. ADDRESS (City, State, and ZIP Code)
8a. NAME OF FUNDING/SPONSORING ORGANIZATION: CRDEC; 8b. OFFICE SYMBOL (If applicable): SMCCR-RSP-B	9. PROCUREMENT INSTRUMENT IDENTIFICATION NUMBER: DAAK11-83-K-0013
8c. ADDRESS (City, State, and ZIP Code): Aberdeen Proving Ground, MD 21010-5423	10. SOURCE OF FUNDING NUMBERS: PROGRAM ELEMENT NO. / PROJECT NO. / TASK NO. / WORK UNIT ACCESSION NO.

11. TITLE (Include Security Classification)
Methods and Measurements of Extinction Properties of Obscurants for Infrared to Millimeter Wave Region

12. PERSONAL AUTHOR(S)
Moeller, K. D.; and Tomaselli, V. P.

13a. TYPE OF REPORT	13b. TIME COVERED	14. DATE OF REPORT (Year, Month, Day)	15. PAGE COUNT
Contractor	FROM 83 Sep TO 86 Dec	1988 May	72

16. SUPPLEMENTARY NOTATION
COR: Robert Frickel, SMCCR-RSP-B, (301) 671-3854

17. COSATI CODES			18. SUBJECT TERMS (Continue on reverse if necessary and identify by block number)
FIELD	GROUP	SUB-GROUP	Aerosol Optics, Extinction by metals
20	03		Millimeter waves/infrared Extinction by carbon
20	06		Millimeter wave spectrometer

19. ABSTRACT (Continue on reverse if necessary and identify by block number)
Extinction and transmission in the far infrared by carbon powder and a variety of metallic powders have been measured. A millimeter wave spectrometer for measuring transmission through aerosol clouds was constructed, incorporating a noise tube as a source. A He-cooled bolometer and a novel beam-splitter for Michelson interferometers of the millimeter and far infrared were developed.

20. DISTRIBUTION/AVAILABILITY OF ABSTRACT	21. ABSTRACT SECURITY CLASSIFICATION
☒ UNCLASSIFIED/UNLIMITED ☐ SAME AS RPT ☐ DTIC USERS	UNCLASSIFIED
22a. NAME OF RESPONSIBLE INDIVIDUAL: SANDRA J. JOHNSON	22b. TELEPHONE (Include Area Code): (301) 671-2914 / 22c. OFFICE SYMBOL: SMCCR-SPS-T

DD Form 1473, JUN 86 Previous editions are obsolete. SECURITY CLASSIFICATION OF THIS PAGE
UNCLASSIFIED

PREFACE

The work described in this report was authorized under Contract No. DAAK11-83-K-0013. This work was started in September 1983 and completed in December 1986.

The use of trade names or manufacturers' names in this report does not constitute an official endorsement of any commercial products. This report may not be cited for purposes of advertisement.

This document has been approved for release to the public.

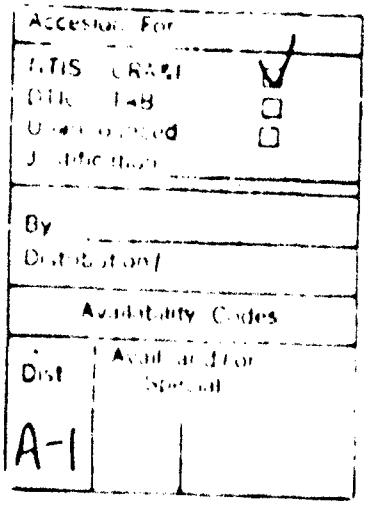

Blank

CONTENTS

LIST OF TABLES

LIST OF FIGURES

METHODS AND MEASUREMENTS OF EXTINCTION PROPERTIES OF OBSCURANTS FOR INFRARED TO MILLIMETER WAVE REGION

Introduction

The work performed under this contract was aimed at the development and construction of a millimeter spectrometer. The spectrometer was intended to be used at a cloud chamber of at least 2 meter path length. Since the aerosol to be measured were not stable for longer than a few minutes, meaningful spectra had to be taken in this time interval.

In the course of this study we measured the far infrared transmission and extinction properties of many particles which might be useful for obscuration purposes. We developed and constructed a dip-stick He-cooled bolometer of superior practical advantages at a NEP of 10^{-12} and invented a new beam splitter for Michelson interferometers of the far infrared and millimeter region. Noise tubes for the millimeter region were employed as sources for Fourier transform spectroscopy in the millimeter region. Finally a millimeter wave spectrometer was constructed showing a S/N ratio of 40 to 50 and could be successfully applied to a cloud chamber. Spectra could be taken within 3 min covering the total millimeter region.

In this report we will first report about measurements on powder particles, then about the beamsplitter and the He-cooled detector, and finally about the noise tube investigation and the millimeter wave spectrometer.

Blank

Far-Infrared Extinction Properties of Metal Powders

The extinction coefficient for metal powders dispersed in a transparent polyethylene matrix has been determined using transmission measurements. Data obtained from three instruments are used to characterize the powders: a grating spectrophotometer for the infrared region, a Fourier transform spectrometer for the far-infrared region, and a CO_2 laser-based photometer system operating at 10.6 micrometers. The laser-based apparatus was incorporated to study sample discs having high concentrations of powder, and thus low transmittance.

The objectives sought in this series of measurements is to investigate the effect of (a) wavelength, (b) particle size and shape, (c) particle concentration, and (d) powder composition on the measured optical properties.

In Table I, we list the physical characteristics of the metal powders under consideration for this series of experiments. All powders were obtained from commercial sources and were used without any subsequent modification or treatment. As can be seen from Table I, powders with a reasonable range of physical characteristics are available commercially. However, the fabrication of controlled, "custom-made" particles should be considered as the next step in this project.

TABLE 1. Physical Properties of Metal Powders Studied

Type	Name	Shape	Size	Apparent Density
Copper	200-U	Flake	44 μ	0.5 g/cc
	R-9427	Flake	44 μ	1.41
	R-9428	Flake	30 μ	0.52
	Leico	Spheres	1-5 μ	
Bronze	Pale Gold Flake		3-5 μ 3-5 μ	(90% Cu/10% Zn)

Measurement error and reproducibility effects continue to be a significant part of this project. Figure 1 presents some typical results of errors introduced by data scatter in transmittance measurements (upper plot) and fluctuation in data resulting from repeated trials on the same series of samples (lower plot). These results were obtained from a bronze powder at a concentration of 1% by weight, but similar behavior was observed for other powders as well.

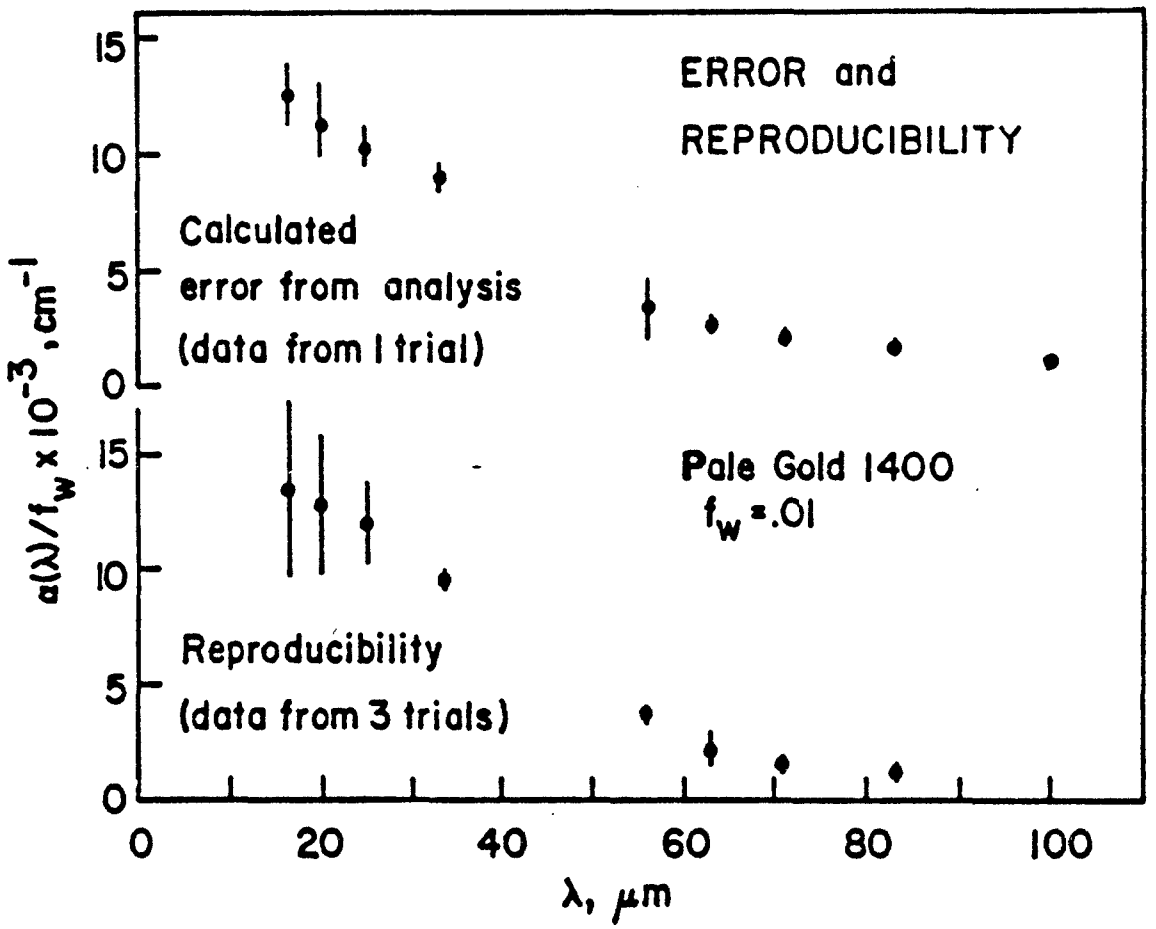

Figure 1. Errors and Reproducibility for Absorption of Pale Gold Particles.

In Figures 2 and 3, we show the wavelength-dependence of the absorption coefficient for a bronze powder and a series of copper powders, respectively. The Pale Gold 1400 graph includes data at four concentrations ranging from 0.1% to 1.0%. The quantity plotted on the vertical axis, α/f_w is a weight fraction normalized absorption coefficient expressed in units of 1000 cm^{-1}.

Here f_w is the weight fraction of metal powder dispersed in the transparent matrix. Figure 2 shows that the absorption decreases with increasing wavelength for all values of f_w, that good agreement between the values obtained from the three methods is quite good, and that the weight-normalized absorption coefficient is essentially independent of concentration. The data point labeled "CO_2" represents a value obtained from the laser photometer method.

In Figure 3, data for four different copper powders is presented. All powders are in the form of flakes, but they differ in their average particle size and apparent density. Density differences here are attributed to the variation in the thickness of the flake. The data in Figure 3 shows that the weight normalized absorption coefficient is independent of wavelength in the region investigated, and has a lower numerical value than does the bronze flake powder.

In Figure 4, we have plotted the absorption coefficient against metal powder concentration, for two wavelengths. There does not appear to be any significant concentration dependence for this data. A listing of experimental data for copper powders is presented in Table II.

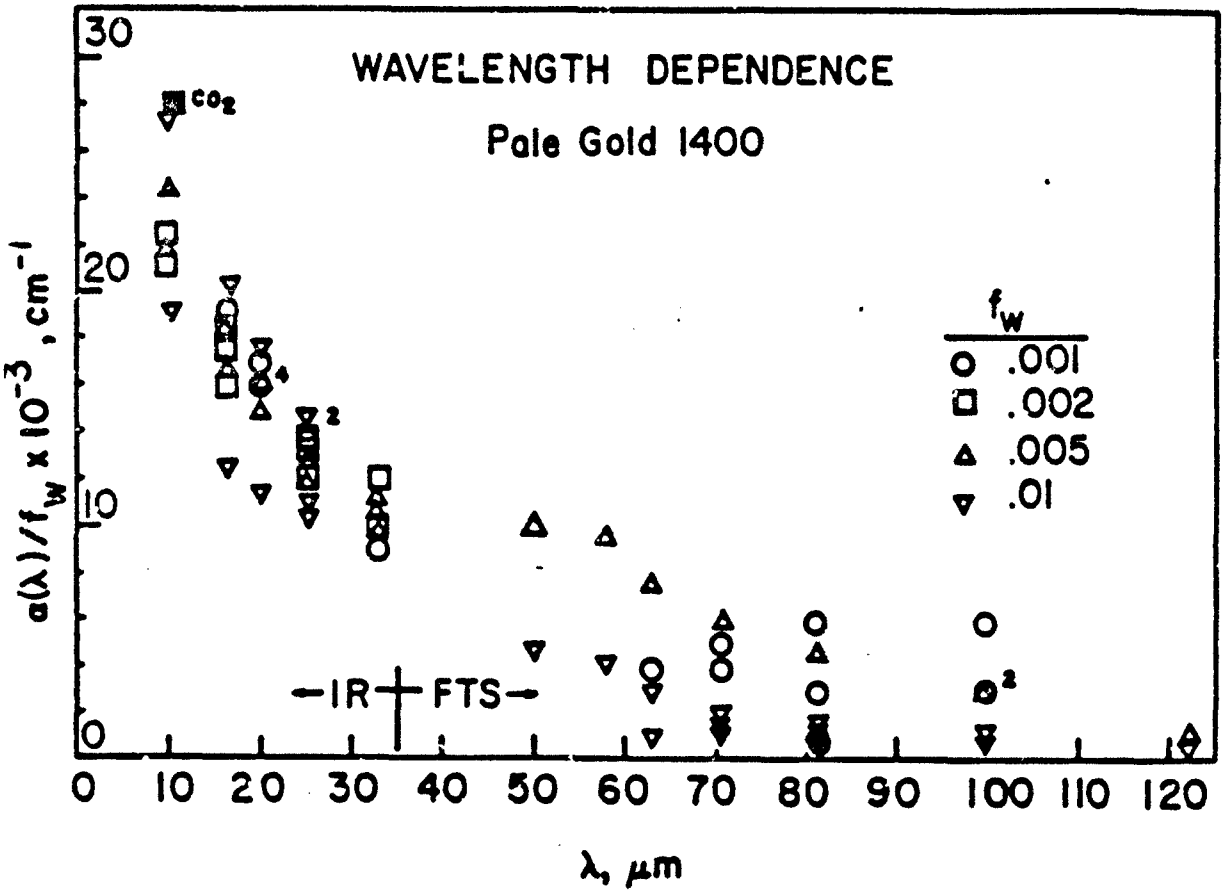

Figure 2. Absorption of Pale Gold Particles.

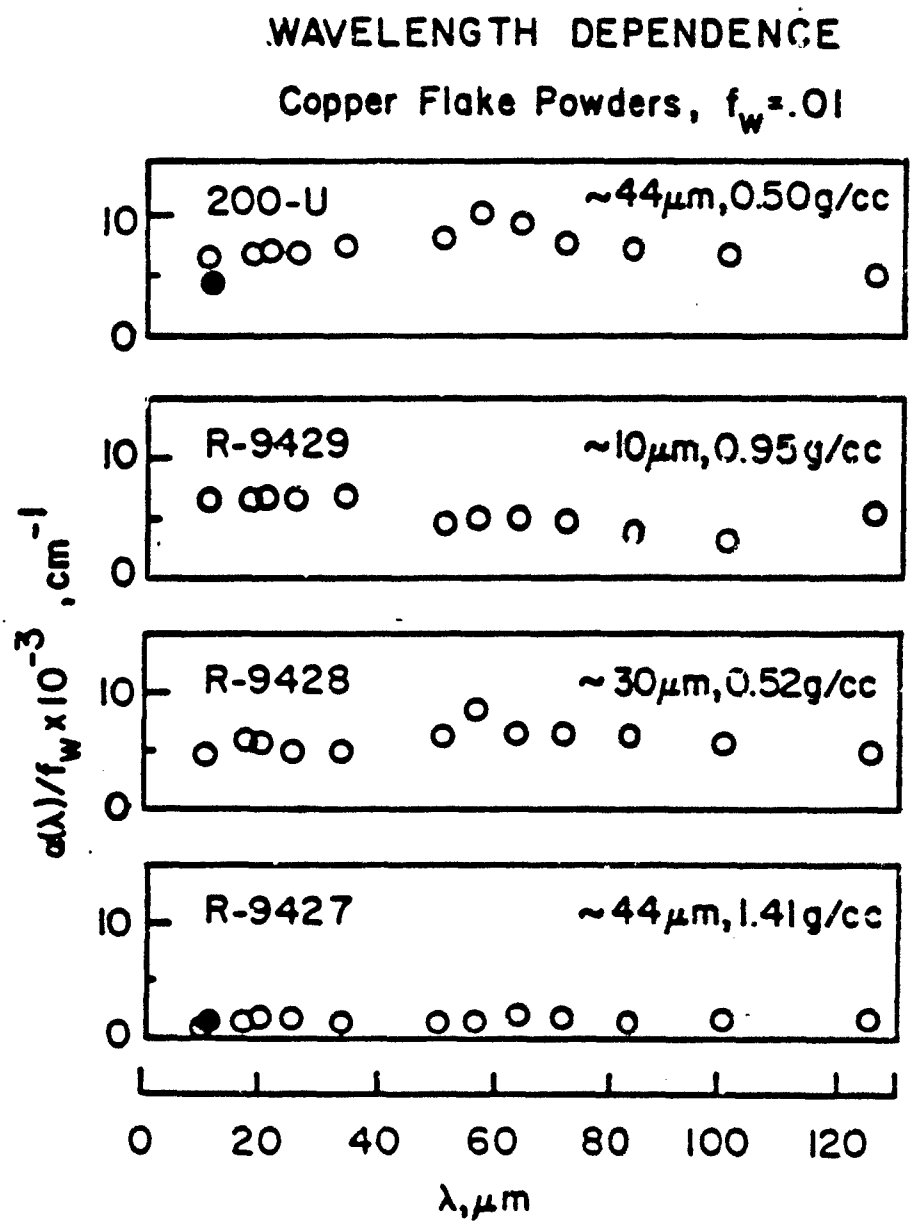

Figure 3. Absorption of Copper Flake Powders.

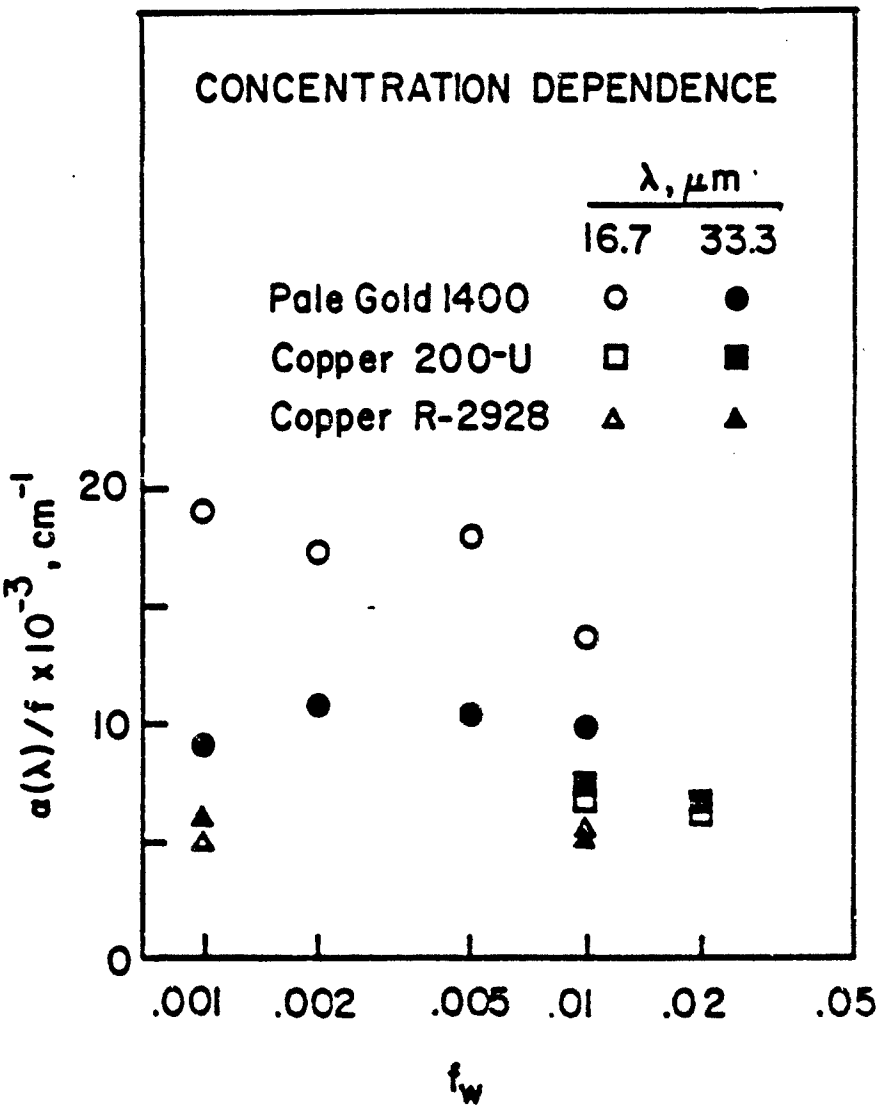

Figure 4. Absorption Coefficient Depending on Concentration for Pale Gold and Copper Particles.

The decreasing absorption from 10μm to 120μm in Pale Gold particles suggests that we are observing the tail of the resonance behavior. According to elementary dipole theory, the resonance should be about two times the average particle size. The nearly flat shape of the copper flake curves does not support this viewpoint.

TABLE 2. Some Experimental Results for Copper Powders

Name	Size (μ)	Shape	f_w	10.0	33.3	100
Leico	1-5	Sphere	.01	1	1	1
			.02	1	1	1
200-U	44	Flake	.01	6.7	7.4	7.2
			.02	5.9	6.5	---
R-9427	44	Flake	.001	0	1	1
			.01	1	1	1
R-9428	30	Flake	.001	3.3	6.3	8.5
			.01	4.8	5.1	5.8
R-9429	10	Flake	.001	4.7	7.7	7.3
			.01	6.5	6.6	2.8

2.0 Attenuated Total Reflection Method for Obtaining the Optical Constants of Powders

2.1 Introduction

The attenuated total reflectance (ATR) method is one of several techniques available for determining the optical properties of materials. It has proven to be particularly valuable for the study of otherwise intractable problems, for example, highly absorbing materials. The method known since its presentation by Fahrenfort,[1] has been used successfully by spectroscopists as a complement to standard absorption and reflection techniques. In those applications, an ATR attachment is mounted in a spectrometer having a broadband source of radiation. More recently, reports of ATR methods using laser sources have appeared. The desirable properties of lasers have resulted in measurements with improved accuracy and sensitivity and have allowed for the undertaking of problems which were previously considered impractical.

We have been interested in measuring the infrared optical constants of powders, particularly highly absorbing powders, and have previously reported the results of specular reflection measurements on a series of black powders[2]. In this work we describe an apparatus used to measure the complex refractive index of a carbon black powder at a wavelength of 3.391 μm and the results obtained. We demonstrate the accuracy of the method by comparing measured optical constants of a liquid hydrocarbon with published results obtained using a different method. Also, we show that the Maxwell-Garnett theory for a composite system can be applied to our measurements.

2.1.1 Experimental Details

2.1.1.1 Background.

The use of ATR methods to determine infrared optical constants has been reviewed by Crawford et al.[3] Briefly, we are interested in the reflectance of radiation at a boundary separating a lossless solid (crystal) from a lossy liquid (sample). If the light approaches the boundary from the lossless medium, the reflected beam will penetrate the sample to a depth approximately equal to the wavelength. This penetrating wave, which is damped exponentially, is called the evanescent wave. The reflectance of this probing wave depends on the optical constants of the crystal n_1 and sample $n_2^* = n_2 - ik$, where k is the absorption coefficient.

The optical behavior at the boundary also depends on the polarization of the radiation. If θ is the angle of incidence at the interface, the reflectance R_s for radiation polarized perpendicular to the plane of incidence is

$$R_s = 1 - \frac{4a\cos\theta}{[a^2+G+(a+\cos\theta)^2]} \quad (1)$$

where

$$a = \{(G^2+4k^2N^4)^{1/2}-G]/2\}^{1/2}, \quad (2)$$

$$G = \sin^2\theta - N^2(1-k^2), \quad (3)$$

$$N = n_2/n_1. \quad (4)$$

These equations, as well as those to be given below, have been given by Hirschfeld.[4] The parallel component of the reflectance R_p is given by

$$R_p = R_s\left[1 - \frac{4a\sin\theta\tan\theta}{a^2+G+(a-\sin\theta\tan\theta)^2}\right] \quad (5)$$

Equations (1) through (5) allow us to obtain the optical constants n_2 and k from measurements of θ, R_s, and R_p. An algorithm for extracting n_2 and k from the measured quantities is as follows:

$$n_2 = n_1\{(X^2+4Y^2)^{1/2}+X/2\}^{1/2}, \quad (6)$$

$$k = \{(X^2+4Y^2)^{1/2}-X/2Y\}, \quad (7)$$

where

$$X = 2a^2-a(F_s+F_p)/2+(1+\tan^2\theta)/2 \quad (8)$$

$$Y = a[(aF_s-a^2-\cos^2)(aF_p-a^2-\sin^2\theta\tan^2\theta)]^{1/2}, \quad (9)$$

$$a = (1-\tan^2)/(F_s-F_p), \quad (10)$$

$$F_s = 2\cos\theta(1+R_s)/1-R_s), \quad (11)$$

$$F_p = 2\sin\theta\tan\theta\ \frac{1+R_r/R_s}{1-R_p/R_s} \quad (12)$$

It has been pointed out by Hirschfeld [4] that the above algorithm is sensitive to round-off errors and that the method cannot be used when the angle of incidence is near 45. This will be seen in results presented below.

Hirschfeld [4,5] has evaluated the accuracy and limitations of several different techniques which utilize the ATR method. The technique chosen here requires a single prism. It has the advantage of being simple to use, although it is less accurate than some of the other techniques.

Figures 5 and 6 are plots of R_s and R_p vs θ generated using the above equations for $n_1 = 4.034$ (germanium) and $n_2 = 1.500$ (approximate value for our samples). The absorption coefficient has been varied from $k = 0$ to $k = 1.00$ in steps as shown. (Fig.5) As expected, for a lossless sample ($k = 0$) both reflectances rise to 1.00 at the critical angle θ_c (here 21.83) and remain there for $\theta_c \leq \theta \leq 90°$. For $k \neq 0$, the reflectance curves change with k.

2.1.1.2 Apparatus.

Figure 7 is a schematic diagram of the apparatus constructed. Radiation from a Spectra-Physics model 120 He-Ne laser L_1 (3.391-μm output only) is chopped at 9.3 Hz, directed into and out of a germanium prism by mirrors M_1, and is detected by a Molectron P1-72 pyroelectric detector. The detector signal is amplified using a Princeton Applied Research model 128A lock-in amplifier and displayed on a Leeds & Northrup strip chart recorder. The germanium prism, isosceles with a prism angle of 140°, is mounted in a goniometer, which allows angular positioning to an accuracy of between 0.05°and 0.20° ,depending upon the angle used. The interface between the germanium prism and sample to be studied is in the horizontal plane so that liquid samples may easily be studied.

A visible He-Ne laser L_2 (Spectra-Physics model 155) is used to align the optical components and set the desired angle of incidence when the removable mirror M_2 is introduced as shown in Fig. 7. The infrared laser (L_1) is mounted in a cradle which rotates about an axis which is colinear with the beam axis. The output beam of this laser is polarized to within one part in one thousand. Rotation of the infrared laser about its longitudinal axis, therefore, allows radiation having either polarization direction to reach the prism-sample interface.

The reflectance values are determined by reading the strip chart reflections with and without the samples on the prism interface and ratioing the resulting numbers.

2.1.1.3 Evaluation of Apparatus and Method.

As a check on the performance of the apparatus and accuracy of the method, we have measured the optical constants of toluene. Toluene was selected as a test material because it has an absorption band at a wavelength very near to the wavelength of the laser line, and thus has a reasonable absorption coefficient k, and because accurate and reliable published values of n and k are available in the literature for comparison. The choice of a liquid for evaluation is obvious since the surface contact problem is not a factor.

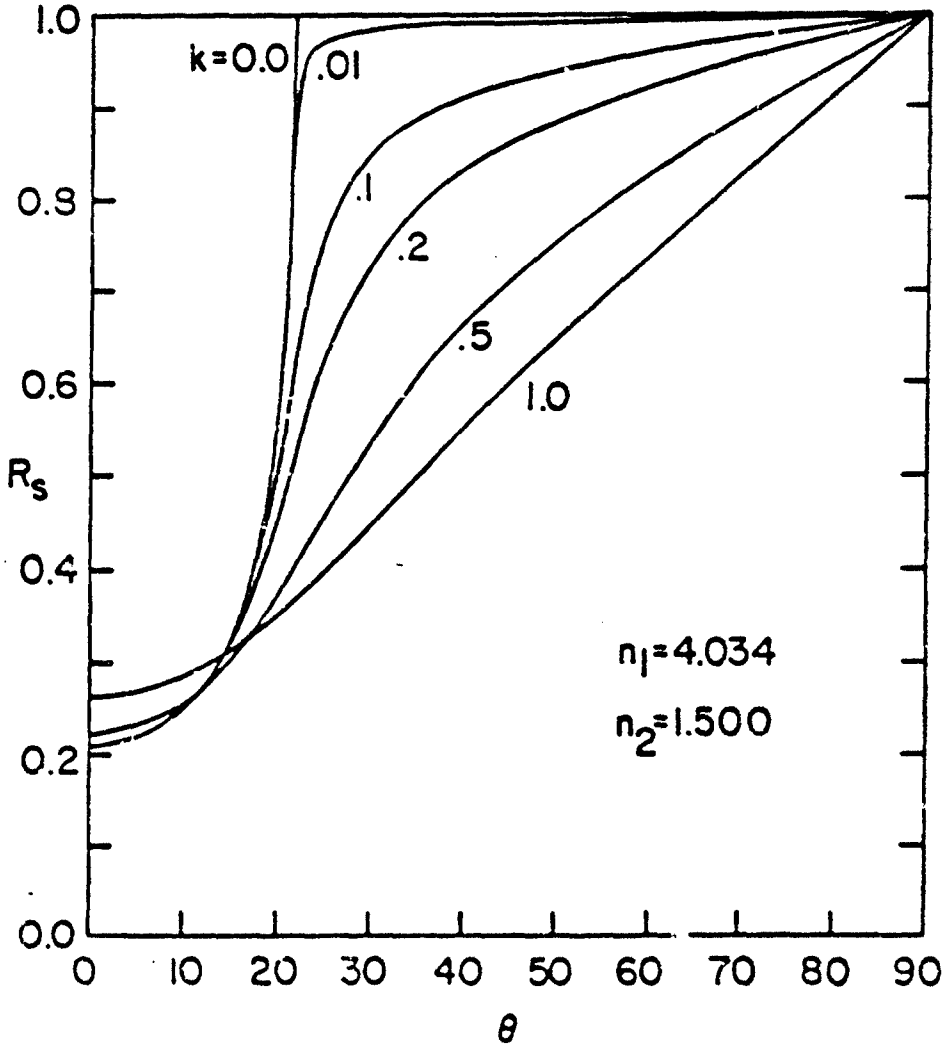

Figure 5. Perpendicular Reflectance vs Angle of Incidence Curves for Various Values of Extinction Coefficients. Critical ngle is 21.83°.

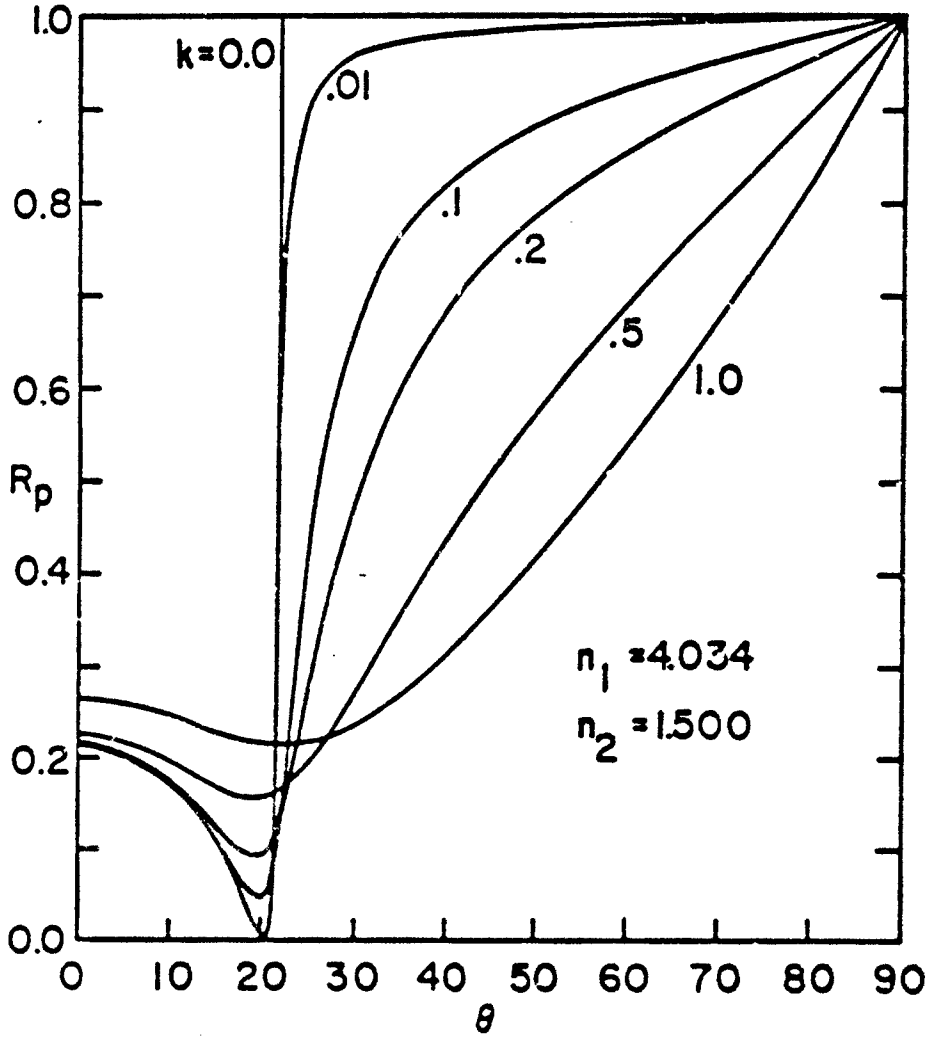

Figure 6. Parallel Reflectance vs Angle of Incidence Curves for Various Values of Extinction Coefficient. Critical Angle is 21.83°.

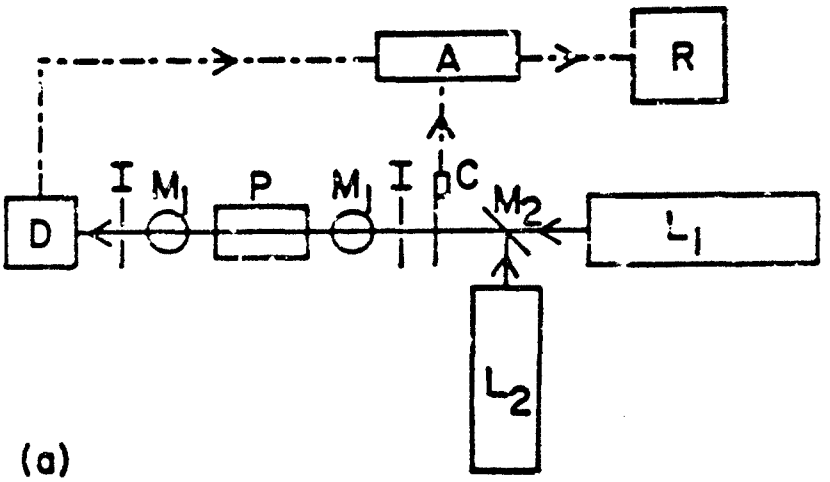

(a)

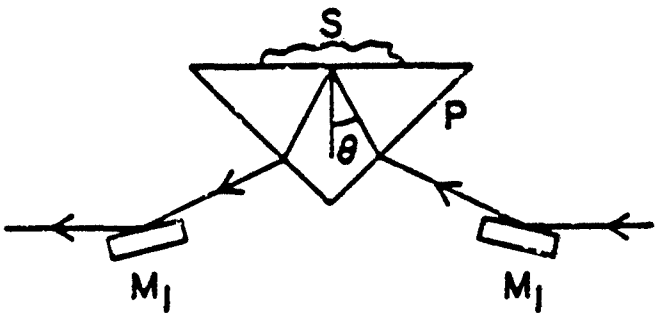

(b)

Figure 7. Schematic Diagram of Apparatus used to Make ATR Measurements. (a) Top View of Components. (b) Side View of Prism Showing Sample S and Path of Laser Beam.

Since the measured quantity in this method is a reflectance, we have presented the results in terms of $R_p(\theta)$ and $R_s(\theta)$. Goplen et al.[6] have reported the results of very careful measurements on a number of organic liquids. Their measurements were made with a grating spectrophotometer using transmittance methods. We have used their published values of n_2 and k measured at 2949 cm^{-1} (3.39 μm), along with n_1 for germanium to calculate $R_s(\theta)$ and $R_p(\theta)$. The results are plotted in Fig. 8 as solid lines and are taken to be the reference values. The open circles in Fig. 8 represent our measured data for toluene on a germanium prism. The agreement is quite good.

The optical constants obtained by Goplen et al. for toluene at 3.39 μm and n = 1.4741 and k = 0.00962. The corresponding values we obtained are n = 1.484 (measured at 19°) and k = 0.015 (measured at 23°). The angles chosen for the measurements were selected on the basis of our error analysis (see below). Our results differ from those of Goplen et al. by 0.7 and 44.0%, respectively. A 44% error in absorption coefficient might appear to be excessive. However, it is approximately the error predicted by an error analysis for a sample with k = 0.01. By comparison, the samples of interest to us in this study have an absorption coefficient k = 0.2. According to our error analysis, we should realize errors in k on the order of a few percent for these samples.

2.1.1.4 Samples.

The objective of this study was to obtain the infrared optical constants of black powder using the ATR method. Transmission measurements on dispersed powder samples are limited in accuracy by low transmittance values and, hence, low signal-to-noise levels. Typical particle loadings (concentration of powder in transparent host medium) for black powders tested spectrophotometrically are limited to 2-5% by weight.

Reflection measurements o compacted pure powder pellets are possible, but reflectances are also low, and the method is subject to other considerations[7]. The ATR method used with a laser source should not be limited by the above problems and should, therefore, offer some advantages. The primary limitation in this method is poor contact between particulate sample and prism. However, this problem may be circumvented by suspending the powder in a liquid of known or measurable optical properties. The surface contact between liquid-powder mixture and prism is then satisfactory, and the optical constants of the powder sample can be extracted from from those of the mixture.

The powder sample investigated in this study was a carbon black (Mogul-L, Cabot Corp., Boston, Mass.). The manufacturer's stated average particle size for this powder is 0.024 μm, but agglomeration effects certainly result in larger-sized clusters. The carbon black powder was mixed with Nujol oil, a refined liquid paraffin commonly used by spectroscopists to prepare mull-type samples. The Nujol was convenient to use, nonvolatile,

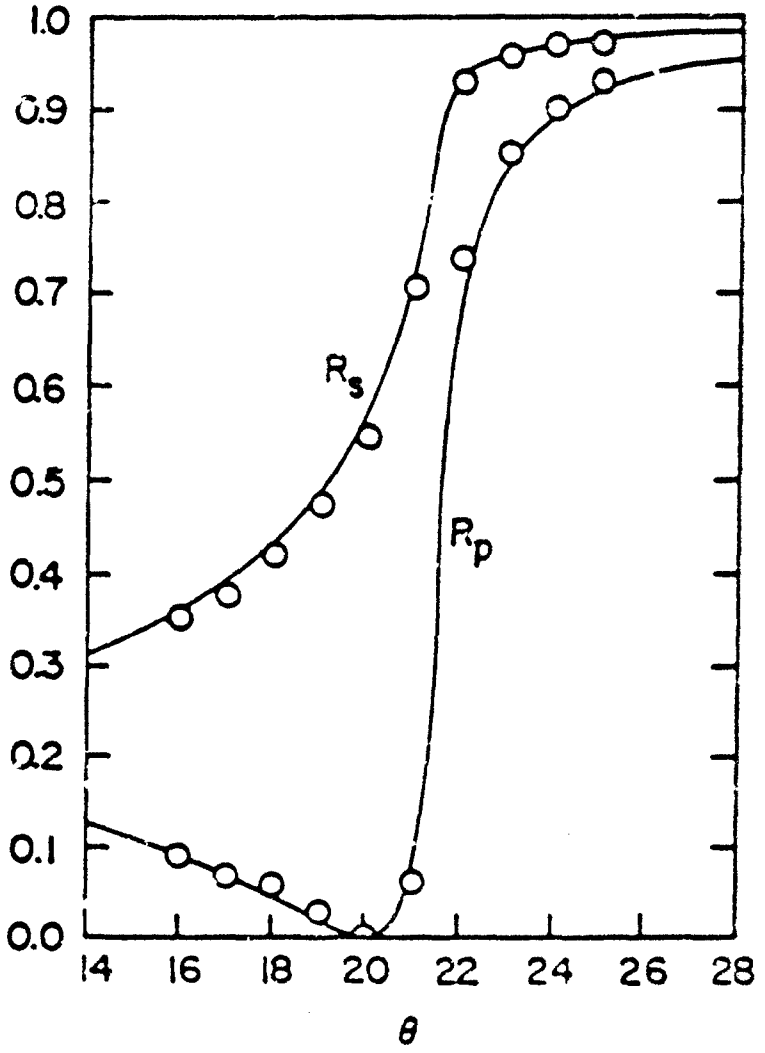

Figure 8. Reflectance Curves for Toluene. Solid Curves are Calculated Data. Open Circles are Experimentel Values.

reasonably pure, and viscous enough to prevent settling out of the carbon black particles during the measurement time. Mixtures of Mogul-L and Nujol were prepared with weight fractions of carbon black from 0 to 50%. Starting with a loading of 40% carbon black, the viscosity of the mixture was such that surface contact problems were encountered. At 50% concentration, the mixture was more pastelike than liquid. No higher concentrations were attempted.

2.1.1.5 Error Considerations.

A method of error analysis similar to that given by Hirschfeld[4] was used here to determine the angle of incidence which would yield the least error in n_2 and k. Values of n_1 = 4.034 (germanium), n_2 = 1.500, and various values of k and θ were used to generate the reflectance values R_s and R_p, and θ were then varied as follows: $\Delta R = \pm .01, \Delta\theta = 0.20°$. These variations in R and r were chosen to be representative of the experimental limitations of the apparatus. The varied R_s, R_p, and θ values were substituted into the algorithm to obtain n_2' and k', the varied optical constants. Finally, the errors $(n_2'-n_2)/n_2$ and $(k'-k)/k$ were calculated and plotted as a function of θ. The results are shown in Figs. 9 and 10 for several values of the absorption coefficient k. The powder suspensions used in this study had k values of $\sim$ 0.1-0.2. Consequently, the optimum values of the angle of incidence used based on Figs. 9 and 10 were between 22 and 25°.

2.1.2 Experimental Results.

Figures 11 and 12 present the results of the ATR measurements on the carbon black suspensions. The values of n and k are given for $0 \leq f_w \leq 0.50$, where f_w is the weight fraction of carbon black. For each sample weight fraction, a minimum of two reflectance measurements were made for each polarization

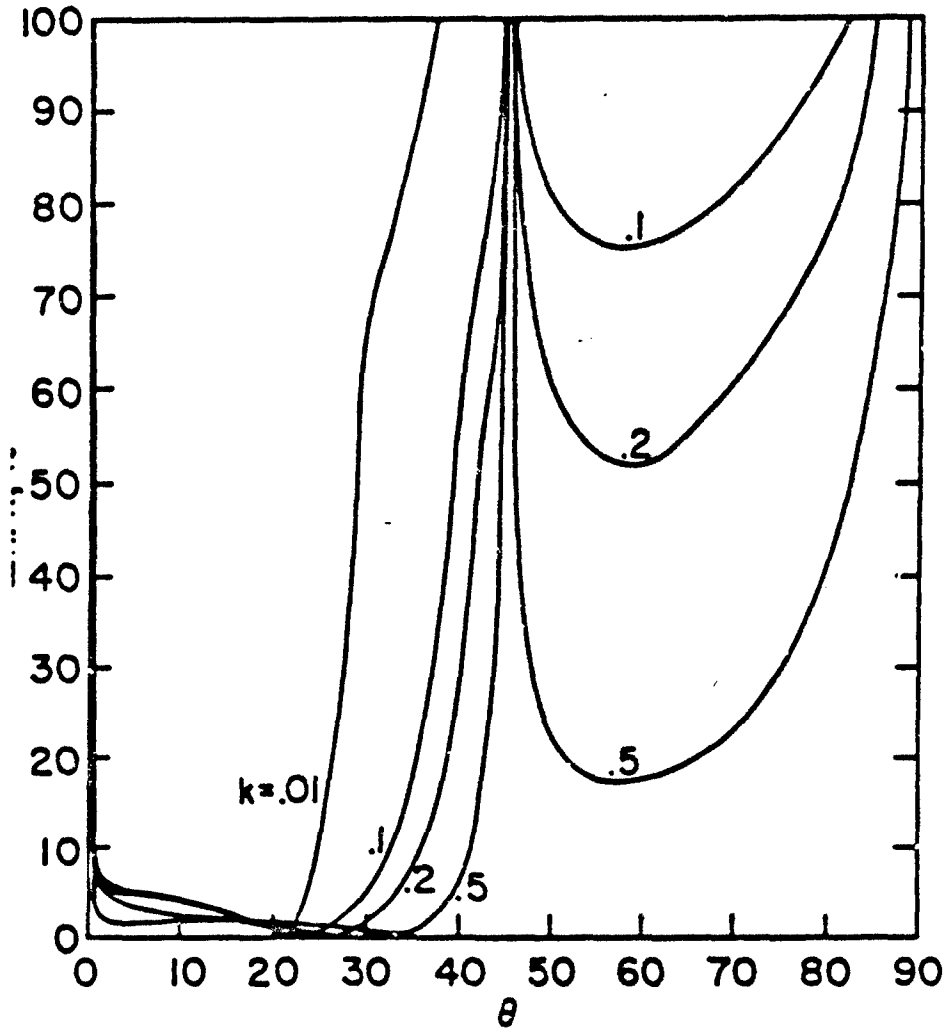

Figure 9. Calculated Error in Index of Refraction. Curves for Various Absorption Coefficients Were Generated Using Algorithm Given in Text and Assuming an Error of ±0.01 in Reflectance Values and ±0.2° in Angle of Incidence.

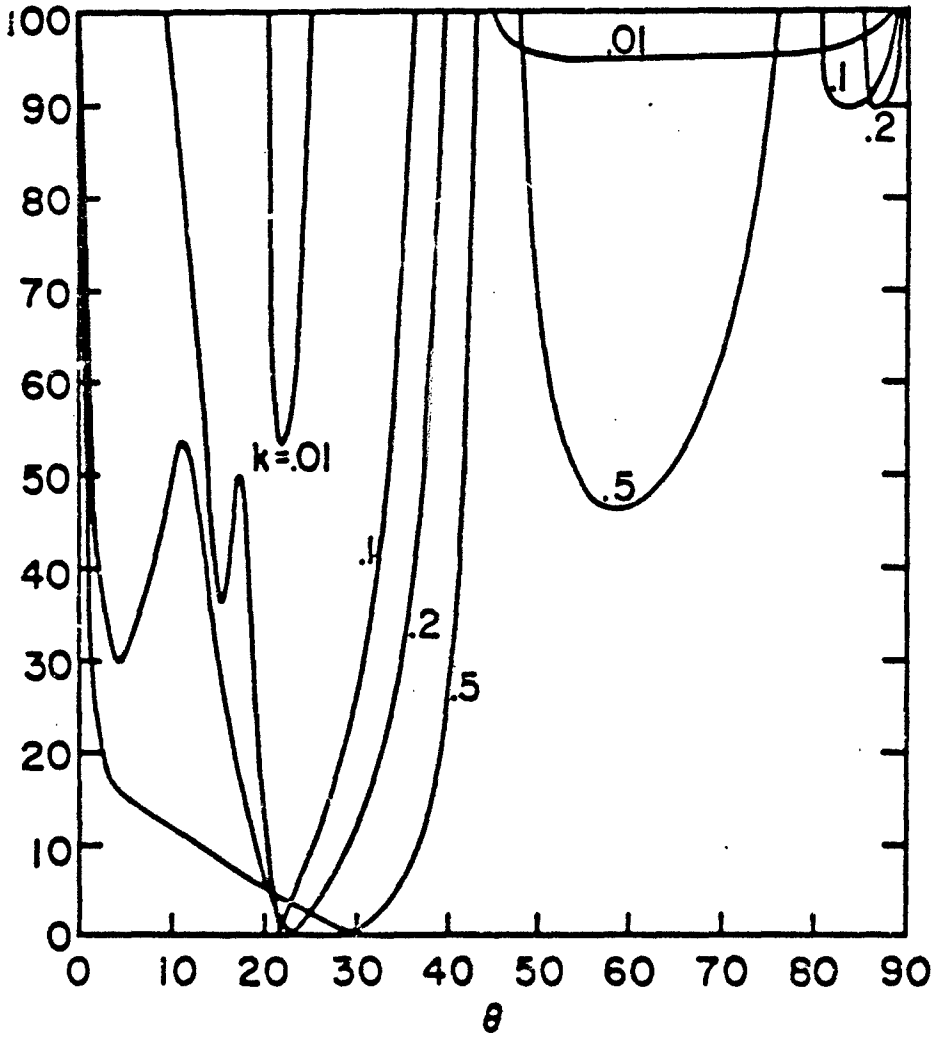

Figure 10. Calculated Error in Absorption Coefficient. (See caption of Figure 9 for details.)

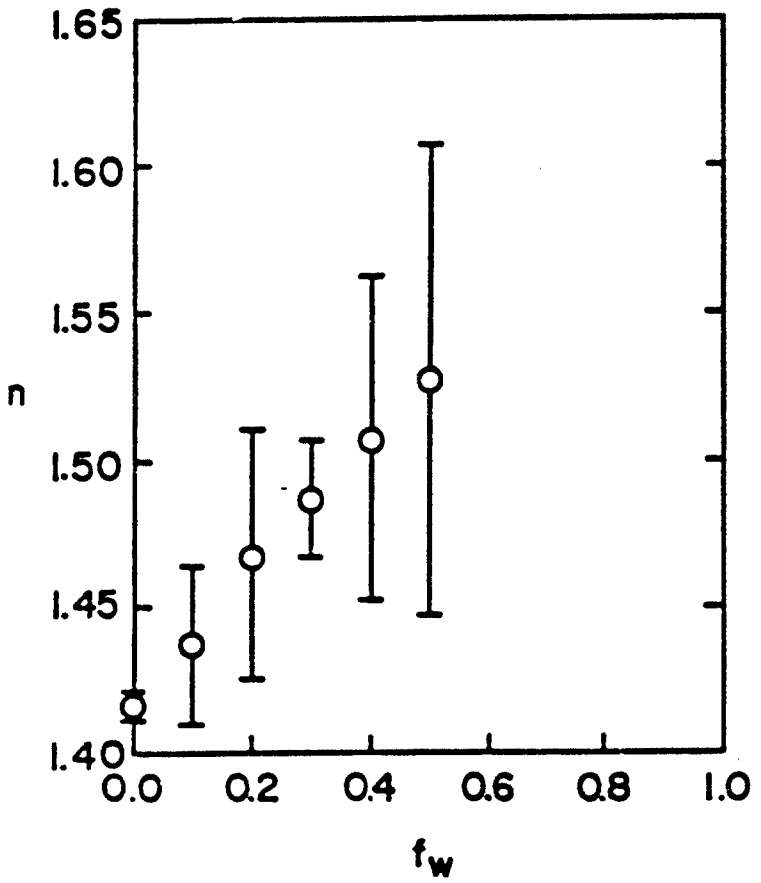

Figure 11. Index of Refraction of Mogul-L Carbon Black Suspension as a Function of Weight Fraction of Powder in Host Material. Error Bars Represent Deviation from the Average Value of Several Measurements.

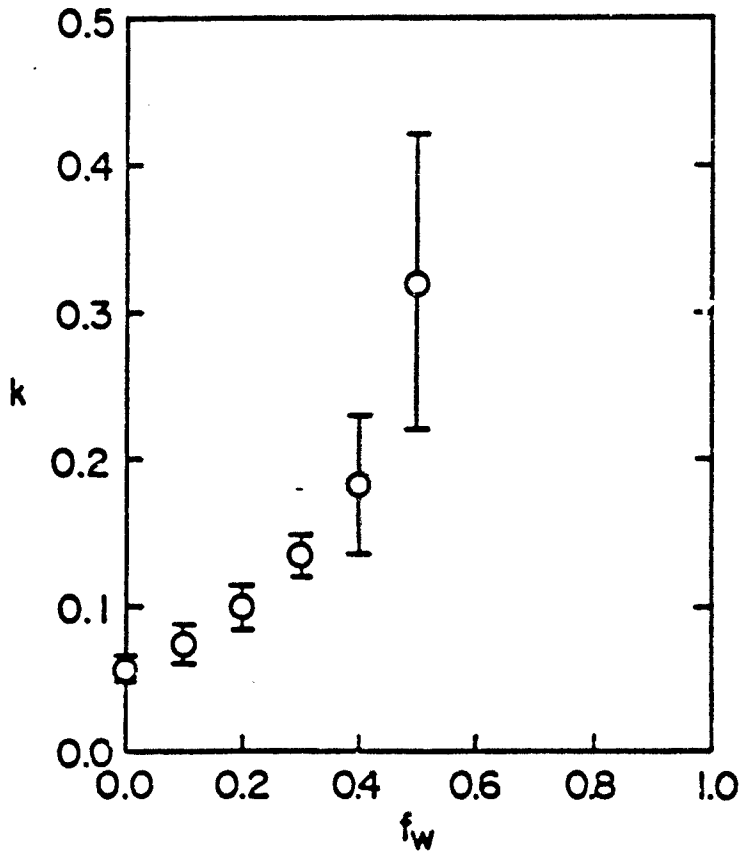

Figure 12. Absorption Coefficient of Mogul-L Carbon Black Suspension as a Function of Weight Fraction of Powder in Host Material. Error Bars Represent Deviation From the Average Value of Several Measurements.

Table 3. Optical Constants of Mogul L Carbon Black Powder at 3.391 μm

	Extrapolated from ATR measurements on powder suspensions; this work	Determined from specular reflection measurements on pressed powder pellet; Ref. 2	Percent difference
n	1.64	1.57	4
k	0.50	0.68	31

direction. The optical constants derived from various combinations of R_s and R_p values were averaged to obtain each data point shown. Deviations from the average values are indicated by the error bars. Not that the scales are not equivalent in Figs. 11 and 12, so that the indicated error bars can be misleading. For example, at $f_w = 0.30$, $\Delta n/n = 1.3\%$, whereas $\Delta k/k = 9.7\%$.

The refractive-index values appear to increase linearly with f_w. A linear regression analysis of the data points gives a correlation coefficient of 0.997. The absorption coefficient data in Fig. 12, by comparison, do not suggest a linear increase of k with f_w, but such a trial linear fit produced a correlation coefficient of 0.923. As will be seen below, this behavior is expected for components with similar permittivities. Assuming that the linear relationships hold for all values of f_w up to unity, the optical constants for the pure powder can be obtained by linear extrapolation. The results, together with values previously obtained, are presented in Table 3.

2.1.3 Discussion.

A correct extrapolation of measurements made on a mixture of the pure powder requires the use of a mixture rule or effective medium theory. Such mixture rules are generally formulated in terms of the permittivity, also a complex quantity. The connection between the permittivity $\varepsilon^* = \varepsilon' - i\varepsilon''$ and index of refraction $n^* = n - ik$ are given by the relations

$$\varepsilon' = n^2 - k^2, \qquad (13a)$$

$$\varepsilon'' = 2nk. \qquad (13b)$$

The simplest effective medium theory, proposed by Maxwell-Garnett,[7] is obtained from the ratio of the volume-averaged electric displacement to the volume-averaged electric field. The result is

$$\varepsilon_{12} = \varepsilon_2 \left[1 + \frac{3 f_v(\varepsilon_1 - \varepsilon_2)}{(1 - f_v)\varepsilon_1 + (2 - f_v)\varepsilon_2}\right] \qquad (14)$$

where $\varepsilon_{12}, \varepsilon_1$ and ε_2 are the permittivity magnitudes of the effective medium suspended component, and host medium, respectively, and f_v is the volume fraction of medium 1. Equation (14) is strictly valid only for small values of f_v (dilute mixtures) and for spherical particles whose diameters are smaller than the wavelength. It can be easily shown that, if

$|\varepsilon_{12}| \approx |\varepsilon_1| \approx |\varepsilon_2|$, both ε_{12} as well as n_{12} and k_{12} depend linearly on f_v for Mogul-L carbon black. The solid line was generated by using Eq. (14) for arbitrary values of f_v but measured values of ε_1 and ε_2. The permittivity ε_2 of the host medium was determined from n and k values obtained using the ATR

apparatus described above. The permittivity ε_1 of the suspended powder was calculated from previously measured optical constants of Mogul-L determined from specular reflection measurements on pressed pellet samples[2] using Eqs. (13a) and (13b). Thus, the solid line represents a calculated or predicted permittivity of the effective medium based upon the Maxwell-Garnett model. The five data points shown in Fig. 13 are for our measured data obtained from various carbon black/nujol mixtures and calculated from Eqs. (13a) and (13b). Weight fractions were converted to volume fractions using a density of Mogul-L (1.25g/cm^3) measured in our laboratory. This density value is different from the apparent density quoted by manufacturer[8] (0.240/cm^3) or that found in the literature for carbon blacks (1.86-2/04 g/cm^3)[9]

The results of Figure 3 show that our measured values of ε_{12} are in very good agreement with the values predicted from the Maxwell-Garnett theory (MGT). The MGT curve exhibits slight curvature and has a pure powder (f_v = 1.0) value of 2.93. A linear regression analysis of the measured data points, including the f_v = 0 point, yields good fit (correlation coefficient of 0.996) and a pure powder extrapolated value of ε = 2.99. These two permittivity values differ by ~2%.

As mentioned earlier, the linear behavior of ε_{12} on f_v is not unexpected since for our materials $|\varepsilon_1| \approx |\varepsilon_2| \approx |\varepsilon_{12}|$. For larger differences between ε_1 and ε_2, the linear approximation becomes progressively less accurate.[2] This explains why, in Figures 11 and 12, both $n(f_v)$ and $k(f_v)$ could be represented by a linear fit with high correlation coefficients (0.997 and 0.923, respectively).

The fact that the carbon black particles are probably not spheres and that relatively high-volume fractions were used appears not to have a noticeable influence on the results. Depending on the grade of material, carbon blacks are produced with a particle size in the range of 10-300μm Fusing and agglomeration results in primary aggregates of random size and shape. Mixing and sample handling may reduce agglomeration effects slightly, but the condition of small spherical and isolated particles assumed in the theory is very probably not met. Very recently, Niklasson and Craighead [10] have measured the optical properties of aluminum-silicon films and analyzed their reflectance data in terms of effective medium theories. Even through electron micrographs of their films showed the presence of non-spherical particles, they obtained good agreement between their measurements and results evaluated from two effective medium theories.

In another recent work, Jennings[11] used the ATR method with a CO_2 laser source to obtain the optical constants of aqueous suspensions of polystyrene spheres. Also using the Maxwell-Garnett theory, Jennings investigated suspensions up to a 30% weight fraction of polystyrene, hardly the realm of dilute mixtures. The polystyrene particles used here, however, were spherical and much smaller than the radiation wavelength.

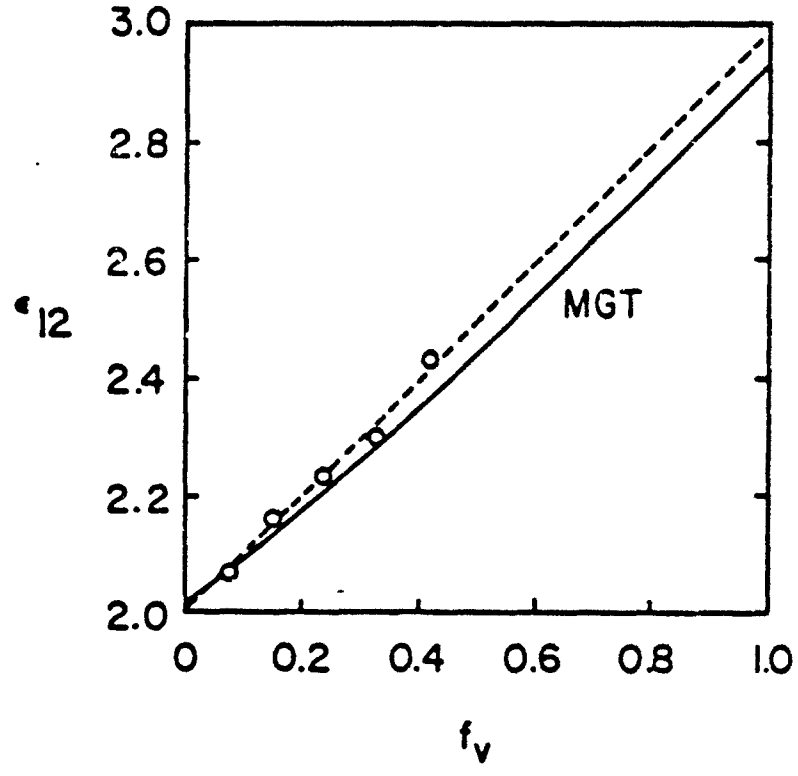

Figure 13. Permittivity of Mogul-L carbon black suspension as a function of volume fraction of powder in host matieral. Open circles are the results calculated from the optical constant data. Dotted line is the linear regression fit of data points. Solid curve is the behavior of equivalent two-component systems as predicted by Maxwell Garnett theory (MGT).

3.0 Capacitive-grid beamsplitters for far-infrared and millimeter-wave interferometers.

3.1 Introduction.

Michelson interferometers are commonly used in Fourier transform spectrometers used for far-infrared spectral measurements. The transparent beam splitter, commonly made from Mylar, is one of the main components in these instruments. The refractive index of Mylar (n = 1.8), however, is only half of that required to produce a beam splitter having optimum reflectance and transmittance properties[12]. A second problem with Mylar beam splitters is that they require a film thickness large enough to produce sufficient reflectance at long wavelengths. A thick film, however, produces a fringe pattern arising from interference effects., Thus, while Mylar has certain properties which make it useful as a beam splitter material (transparency, mechanical stability, ease of handling), it also has some disadvantages.

To overcome these problems and allow for operation of the instrument over a large wavelength range, commercial far-infrared spectrometers use a series of beam splitters. Some manufacturers provide a positioning device that allows one of several beam splitters to be inserted into the optical beam without breaking the vacuum. However, to obtain precise far-infrared spectra, it is desirable to obtain the spectrum using a single beam splitter which covers at least several octaves of the spectrum.

A Michelson interferometer with a Mylar beam splitter operates as an amplitude division interferometer. The lamellar-grating interferometer by comparison, uses wave-front division. The operation of a lamellar-grating interferometer suggested the attempt to construct a wave-front dividing beam splitter for the Michelson interferometer. The device constructed is called a capacitive-grid beam splitter. As used here, a capacitive grid is a patterned deposition of metal (copper) on a (6 μm) Mylar substrate so that the metallic regions are isolated. An example of a capacitive cross grid pattern is found in Fig. 1(b) of Ref. 13. A beam splitter having a pattern composed of a regular array of metallic dots (see Fig. 14) has been used to obtain far-infrared spectra. By a proper choice of dot diameter, such a beam splitter can be used over a large spectral region and is suitable for practical applications.

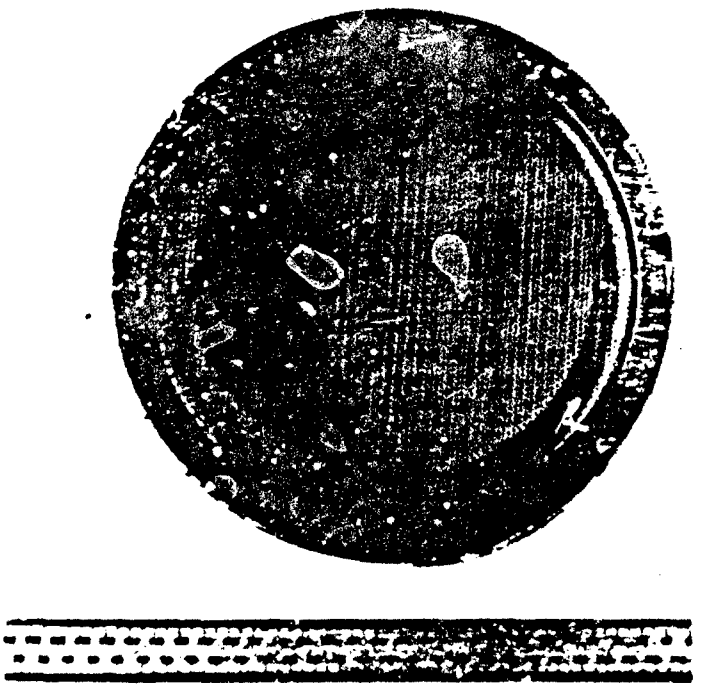

Figure 14. Capacitive Grid Beamsplitter. Opaque dots are copper depositions of ∿ 1.6mm diameter arranged in a lattice of constant ∿ 2.5mm. Substrate is 6μm thick Mylar film.

3.2 Theory.

A beam splitter constructed having a gratinglike pattern of opaque and transparent regions with grating constant a which is larger than wavelength λ will produce diffraction effects. If we compare a lamellar grating with a given λ/a ratio to a grating-type beam splitter with the same λ/a used in a normal Michelson interferometer, we see that the main disadvantage to the latter comes from the fact that the radiation is incident twice on the beam splitter. This means that diffraction also occurs twice. To compare the two types of diffraction beam splitter we consider a lamellar grating as shown schematically in Fig. 15. Monochromatic radiation is incident at some angle to the grating normal so that 50% is reflected from the upper surfaces of the structure (III') and 50% is reflected from the lower, moving, and interpenetrating surfaces (IV'). For a given displacement x of one surface relative to the others, beams III' and IV' will undergo destructive interference for the zero-order position shown. The energy is then distributed into the first-order position (not shown). Zero- and first -order lights have a phase difference of 180°.[1] Conversely, when the zero-order pattern is at a maxima due to constructive interference of rays III' and IV', no energy is distributed in the first-order positions. Thus the distribution of energy alternates between zero and first orders. The next higher orders can be neglected because of their low intensities.

In a Michelson interferometer (see Fig. 16) using a capacitive grid as a beam splitter, radiation is diffracted into zero and first order for the first pass through the beam splitter (higher orders are again neglected). Most of the light in first order is lost as a result of being diffracted away from the optic axis of the system. For the second pass, the zero order of the two beams resulting from the first dividing process undergo interference in the directions of the detector and source as in the lamellar-grating case. When the zero order in the direction of the source is undergoing constructive interference, the corresponding zero order in the direction of the detector is undergoing destructive interference. The first-order pattern in the detector direction has zero intensity, but the first-order pattern in the source direction has a nonzero intensity. This division will again result in losses.

The similarity between the lamellar- and diffraction-grating beam splitter can be exploited to analyze the restrictive condition on the on the cutoff wave number ν_c. Consider a lamellar grating with periodicity a used in an interferometer configuration with an aperture diameter s and collector optic focal length F. The cutoff wave number for which first-order radiation enters the exit slit is[12].

$$\overline{\nu}_c = F/as. \qquad (15)$$

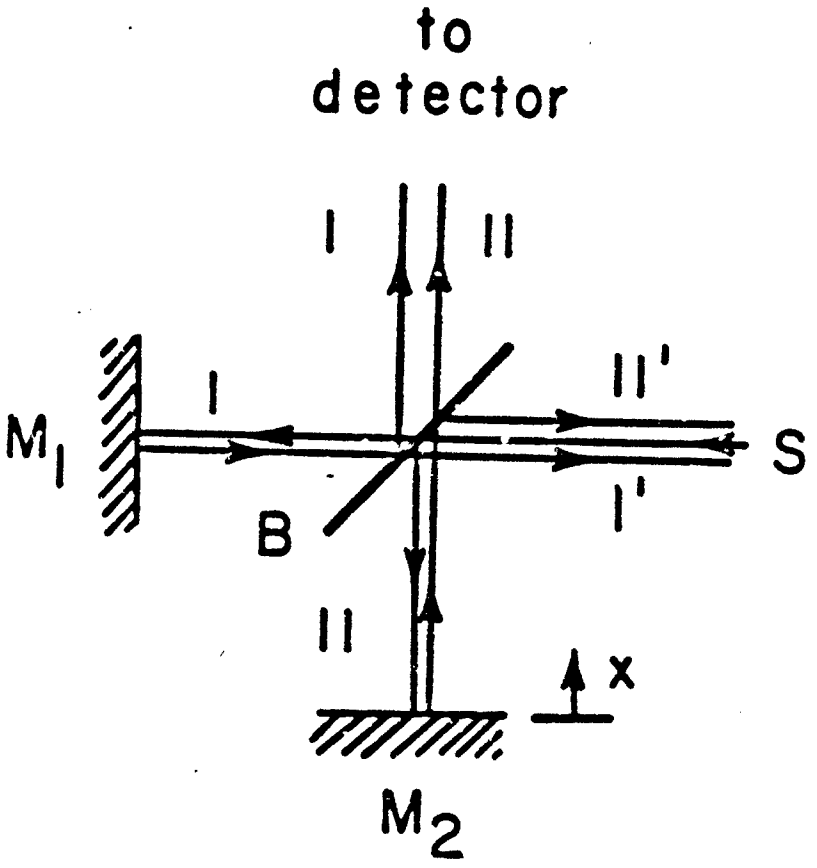

Figure 15. Schematic Diagram of Michelson Interferometer. S is radiation source, B is beamsplitter, M_1 is stationary mirror, M_2 is movable mirror. Light paths I and II, etc. are shown displaced for pictorial reasons only.

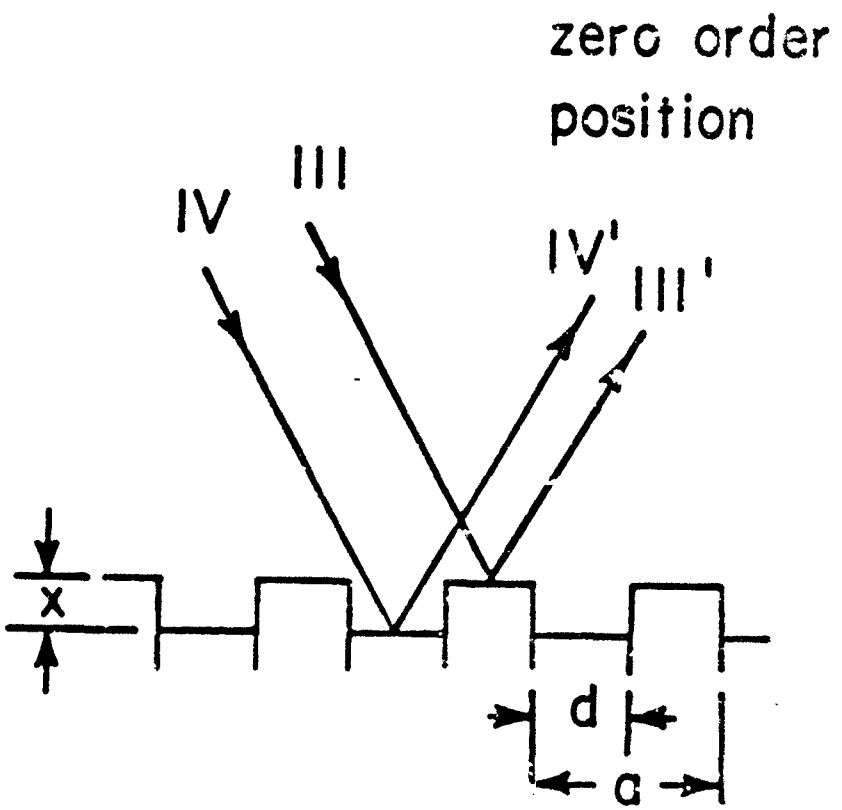

Figure 16. Schematic Diagram of Lamellar Grating, side view. a is grating constant, d is step width and x is relative displacement of interpenetrating surfaces.

This condition places an upper limit on the value of s, which will ensure maximum efficiency. For wave numbers $>\overline{\nu_c}$, radiation from higher orders enters the exit aperture and correspondingly lowers the efficiency.

For the diffraction-grating beam splitter used in a Michelson interferometer, Eq.(1) may be used. If the grating constant a is modified to account for its projected periodicity in a plane perpendicular to the optic axis of the interferometer arm (a factor of $1/\sqrt{2}$ for 45° tilting of the beam splitter), the cutoff wave-number condition becomes

$$\overline{\nu_c} = f/(a/\sqrt{2})s. \qquad (16)$$

The numerator f must now be taken as the beam splitter to exit slit distance if a focusing Michelson interferometer is used (see Fig. 17).

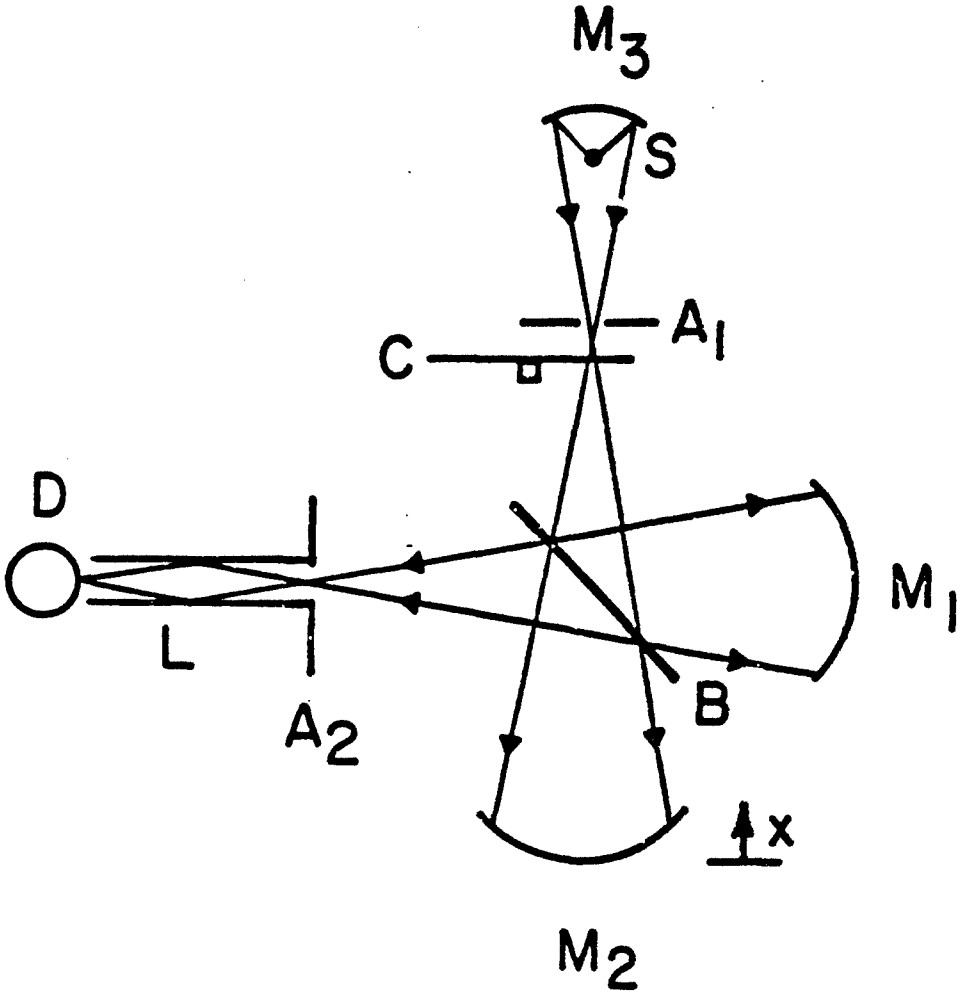

Figure 17. Schematic Diagram of Michelson Interferometer Using Focusing Mirrors.
M_1 and M_2 are spherical mirrors (focal length 9 inches), B is beamsplitter, C is chopper, S is source (mercury lamp), A_1 and A_2 are entrance and exit apertures, L is light pipe and D is detector.

3.3 Experimental Results.

A comparison of interferograms obtained using the gratinglike beam splitter and the dot-pattern beam splitter showed that the latter produced better interferograms. These two devices were compared by judging the ratio of the maximum of the interferogram to its average level. This ratio should be 2:1. It was found that this ratio could be obtained with 2-D dot pattern for larger aperture openings than with the gratinglike beam splitter. This can be understood from spatial coherence considerations.

For the spectra shown in Figs. 18-22, dot-patterned beam splitters were used. These beam splitters were produced by vacuum evaporation of copper through a mask onto a 6 μm thick Mylar film substrate. Circular dot patterns were selected because commercially manufactured metal masks were readily available having various dot sizes and interdot distances. Thus it was possible to vary the area of the dots and the ratio of opaque to transparent areas of the beam splitter. The metal dots on the Mylar substrate had a thickness of 4000-5000 A. Copper was evaporated on either one or both sides of the Mylar film and is so indicated in the caption of each figure. Following vacuum deposition of the metal dots, the Mylar substrate was stretched on a circular drumhead-type holder (see Fig. 14). All beamsplitters were investigated using a Michelson interferometer with focusing mirrors (Fig. 17). This instrument described earlier [14] was operated under vacuum conditions. A dip-stick bolometer described elsewhere was used as a detector. Components inserted into the optical beam of the spectrometer included a 2-mm quartz lens located just above the detector element, a black polyethylene short-wavelength filter, and a clear polyethylene vacuum window. For a comparison of the different beam splitters, the instrument was equipped with circular entrance and exit apertures, each having a diameter of 19mm. This choice was made for practical considerations resulting from the spectrometer geometry. The beam splitter-to-exit aperture distance on-axis was 30cm. The interdot distance of the beam splitter having nominal 3.3 mm diam dots was 5.5 mm. As an example of the use of Eq. (16), we calculate the cutoff wave number for an aperture diameter of 19 mm. The result is $\overline{\nu}_c = 300/[(19)(5.5/\sqrt{2})] \approx 40\ cm^{-1}$. If the aperture size s is increased, the cutoff wave number is reduced resulting in more cancellation in the wavelength range under consideration. Since clear Mylar beam splitters do not have this restriction, they have from this point of view an advantage. However, for the longer wavelengths for which the patterned beam splitter has been designed, this advantage vanishes.

Figures 18-22 show the spectra obtained with a 50 um transparent Mylar 3.3 mm diam double-coated dot pattern, 1.6 mm diam. single-coated dot, and 1.0-mm diam single-coated dot beam splitter, respectively. The intensity scale is in relative units but is the same for all cases. All spectra were obtained using the same resolution, recording time, and time constant.

The weak absorption bands shown at the same wave numbers in Figs. 18-22 are due to interference fringes caused by the polyethylene window. The quartz band at 127 cm^{-1} can also be seen. The stronger bands in Figs. 18 and 20 are due to interference fringes caused by the Mylar film.

We have also investigated beam splitters having 1.0 and 1.6 mm dot diam. produced on 6 μm Mylar substrates. The beam splitter had clear-to-opaque area ratio of 1.9, and coated on one side only. The spectra is shown in Figs. 21 and 22.

3.4 Discussion and Conclusions.

In most treatments of beam splitters, the material is considered to be optically lossless. Naylor et al[14] have accounted for the effect of absorption by Mylar in beam splitters. They calculate the reduction in modulation efficiency of a 100 μm Mylar beam splitter as a function of wave number for several angles of incidence. The effect of absorption is clearly seen and is more significant for the higher wave numbers. We have investigated a 225μm thick translucent beam splitter and observed no appreciable transmission for wave numbers above 80 cm^{-1}. By comparison, clear Mylar transmitted no radiation above 200 and 120 cm^{-1} for the 50 and 175μm thickness, respectively. A dotted beam splitter prepared on a 6μm Mylar transmitted up to 200 cm^{-1} as a consequence of the thin substrate.

The capacitive-grid beam splitters described in this paper have the advantage of not producing interference fringes over a considerably large far-infrared spectral region. They yield approximately the same peak transmission as do the clear Mylar beam splitters. In addition, they are relatively easy to produce and eliminate the need to change beam splitters for investigation in extended spectral regions.

4.0 Dip Stick Bolometer

Ten years ago we developed a dip stick detector for the far infrared[15]. The detector element was mounted at the end of an evacuated light pipe. The light pipe was dipped into a He storage dewar. The light from the spectrometer was conducted through the light pipes to the detector. A thin wire was conducting the signal to a preamplifier mounted outside of the detector housing. A schematic of these arrangements are shown in Fig. 23. The detector was a doped-Ge photoconductive detector.

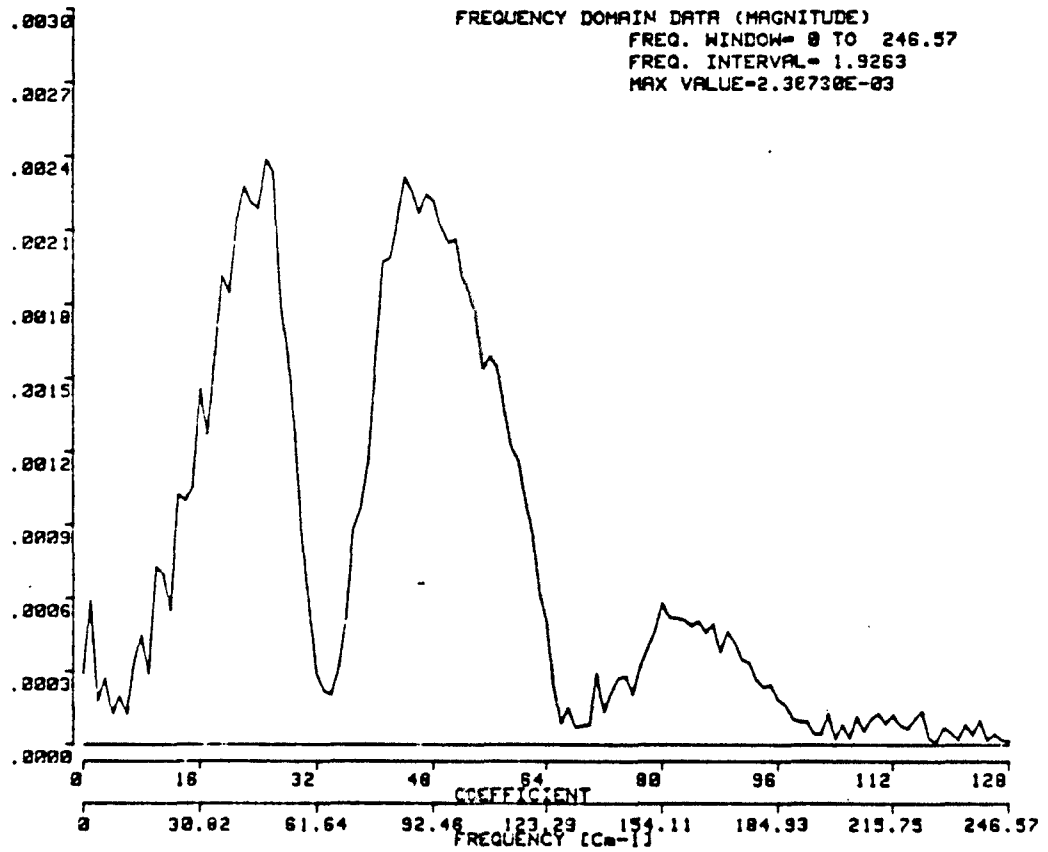

Figure 18. Spectrum obtained with 50-μm thick Mylar beam splitter. The strong band at 70cm^{-1} is a Mylar interference fringe. The weak bands are interference fringes caused by the polyethylene window. A mercury lamp, 2-mm quartz lens, and black polyethylene filter were used.

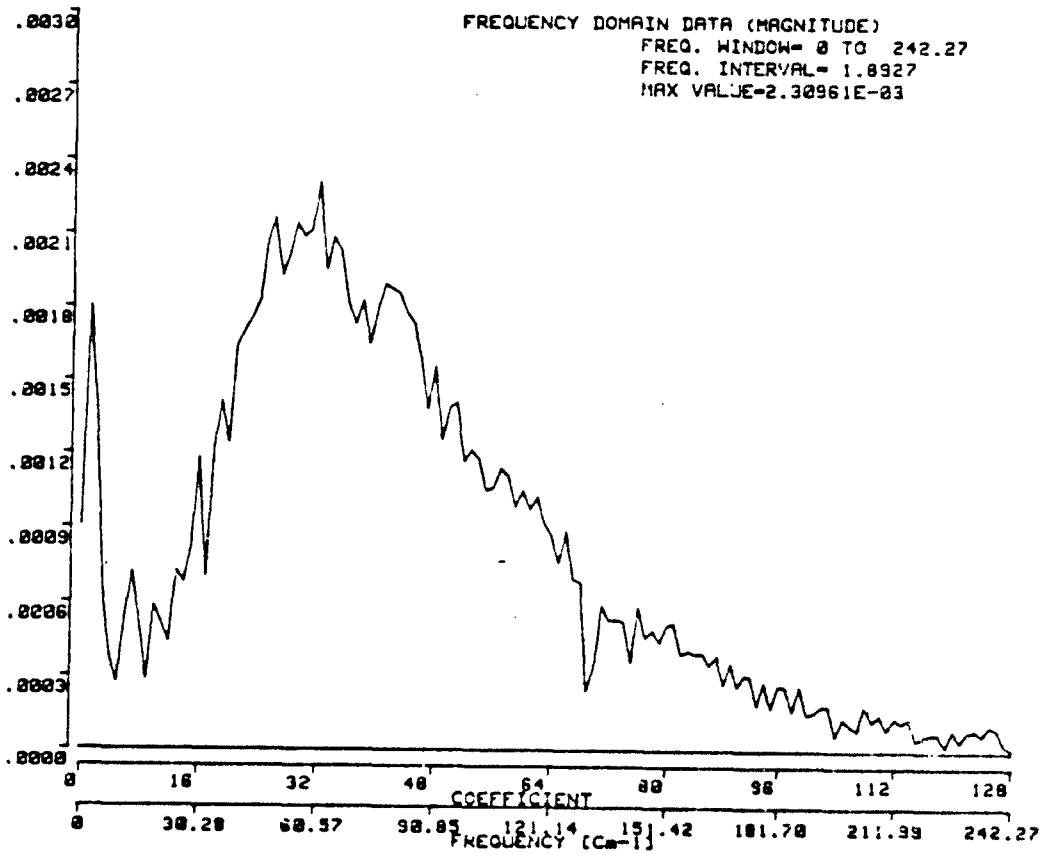

Figure 19. Spectrum obtained with beam splitter having 3.3-mm diam. copper dots on 6-μm thick Mylar arranged in a lattice of constant 5.5 mm. The weak bands are interference fringes caused by the polyethylene window. A mercury lamp, 2-mm quartz lens, and black polyethylene filter were used.

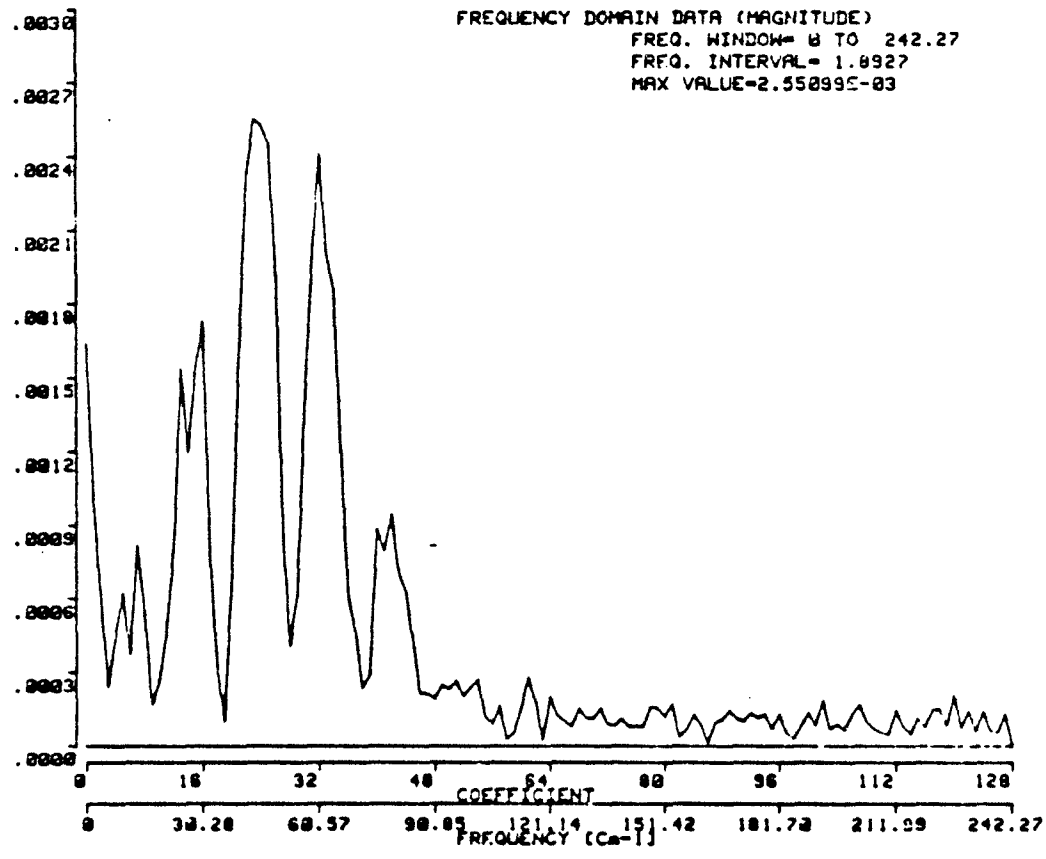

Figure 20. Spectrum obtained with 175-μm thick Mylar beamsplitter. The strong absorption bands are interference fringes caused by the Mylar. The weak bands are interference fringes caused by a polyethylene window. A mercury lamp, 2-mm quartz lens, and black polyethylene filter were used.

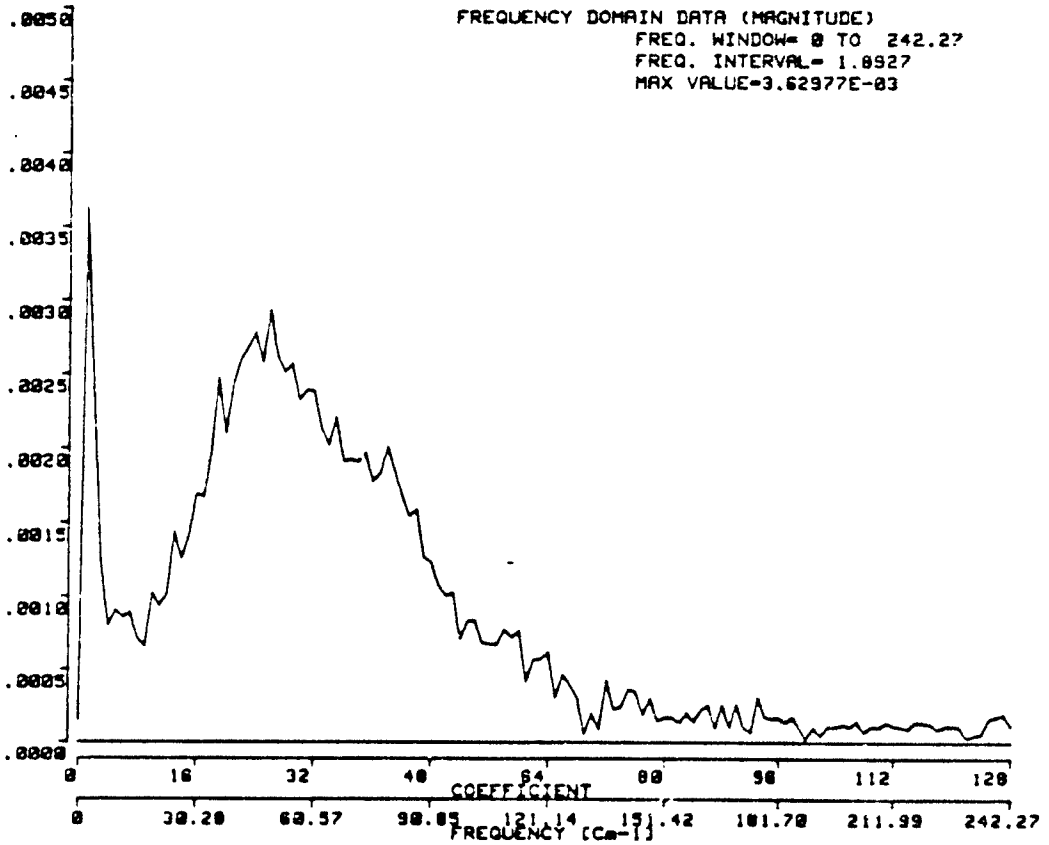

Figure 21. Spectrum obtained with 1.6-mm dot diam. beamsplitter coated on one side only. The dot-to-dot distance is 2.5 mm. The weak absorption bands are interference fringes caused by a polyethylene window. A mercury lamp, 2-mm quartz lens, and black polyethylene filter were used.

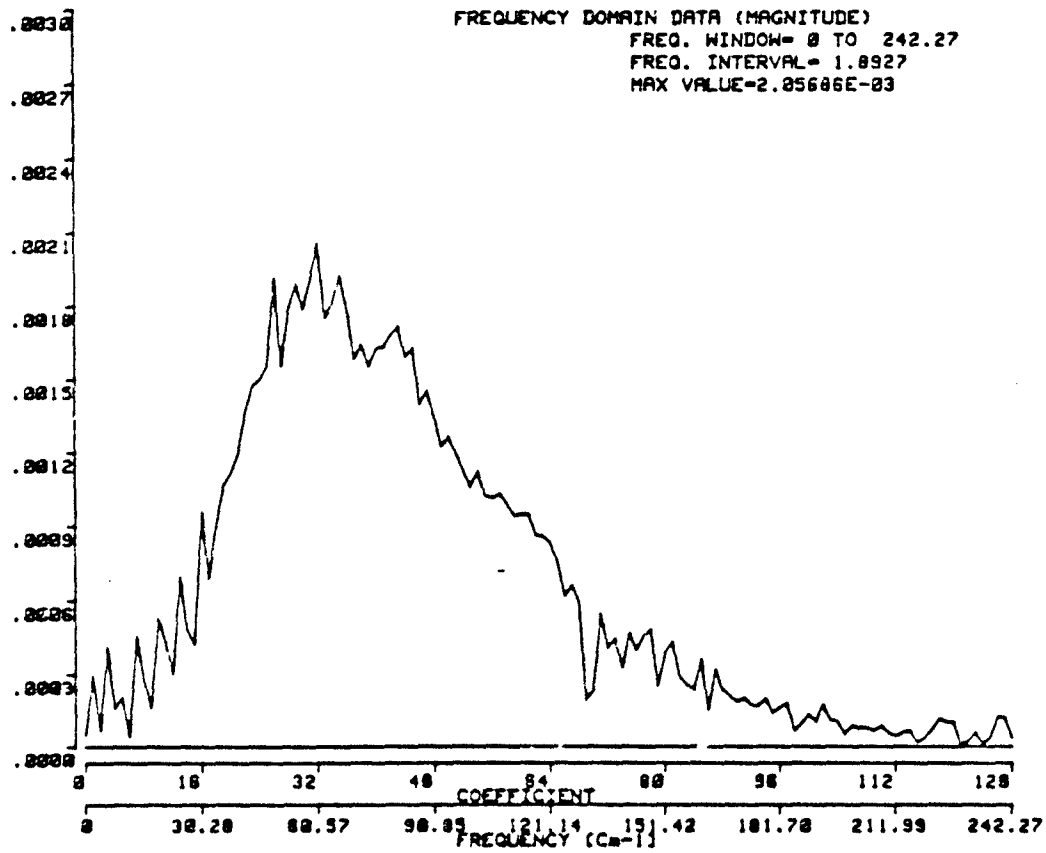

Figure 22. Spectrum obtained with 1.0-mm dot diam. beam splitter coated on one side only. The dot-to-dot distance is 1.3mm. The weak absorption bands are interference fringes caused by a polyethylene window. A mercury lamp, 2-mm quartz iens, and black polyethylene filter were used.

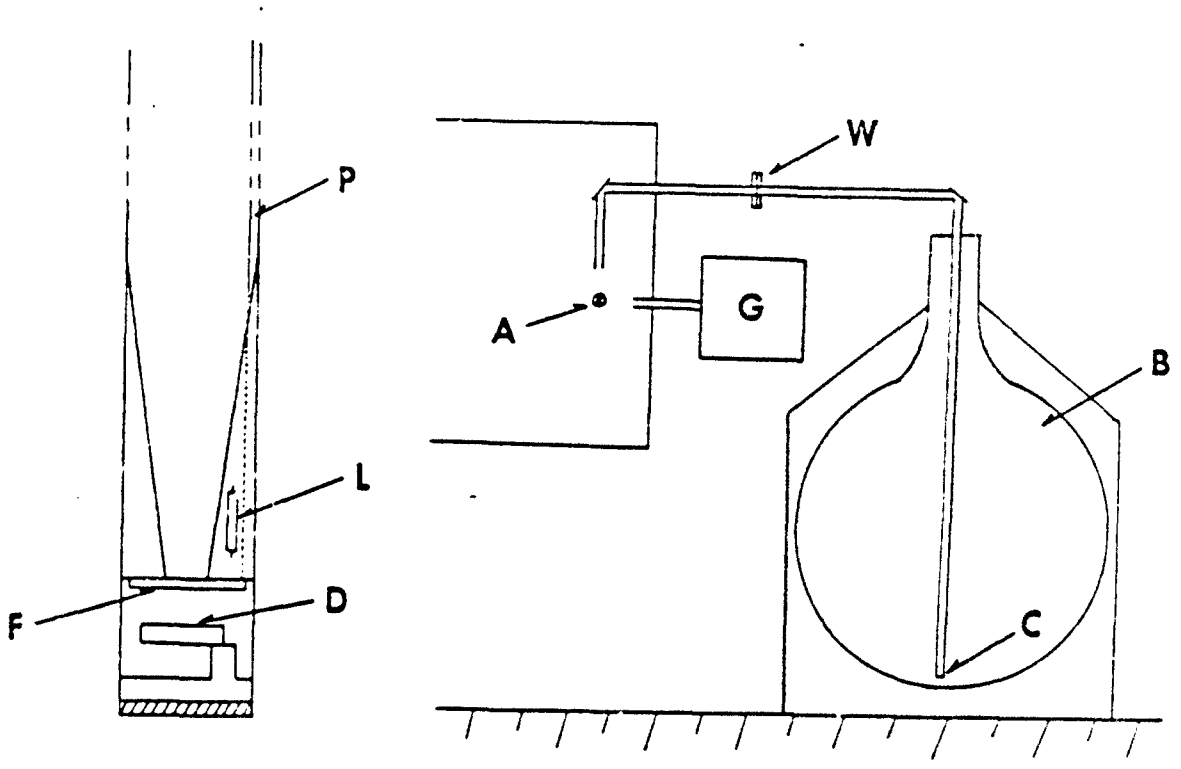

Figure 23. Mechanical arrangement of dip stick detector and He storage dewar.

P - pipe
F - filter
L - load resistor
D - detector
A - movable mirror
W - window
G - Goley detector
B - helium can
C - detector position

To apply the same arrangement to a bolometer was much more difficult. The bolometer needs a high vacuum and a good contact to the helium bath. The detector was sealed with a crystal quartz window in contrast to a polyethylene window used before. The bolometer element was mounted directly on the plug at the end of the light pipe for good contact to the helium. A quartz lens with a black polyethylene filter were mounted on the plug to act as cooled background radiation filter. The filter elements were produced according to recipes from NASA Goddard Space Flight Center (Dr. Moseley).

The details for mounting of the components and the soldering of the plug had to be determined experimentally. At present we use detectors of an NEP of 10^{-12}, as good as they can be when pumping on the helium is not possible.

5.0 Noise Tube Sources for the Far IR and Millimeter Region.

5.1 Introduction

Noise tubes are used as reference and calibration source in microwave and millimeter wave spectroscopy. A gas discharge tube is mounted with respect to a wave guide under a small angle so that radiation is coupled into the waveguide. If the noise tube is used with an optical spectrometer an antenna horn is used[16].

Two different types of noise tubes were investigated. One was model TN-167 for the 90-140 GHz region, manufactured by C. P. Clair and Co. See Fig. 24. The other was specially made for us and contained the same gas at the same pressure of the above noise tube. The gas was contained in a 1" diameter fused quartz tube of 1mm wall thickness. Both noise tubes were operated with a regulated power supply (C. P. Clair & Co.) with currents between 50mA and 125mA. According to specifications, the noise tube should emit more longer wavelength radiation when operated with lower current.

5.1.1 Spectrometers and Detectors

The study of the noise tube emission and the comparison to mercury lamps was conducted with a lamellar grating of 1.8cm grating constant and f/2 optics and a Nicolet FIR-FT spectrometer.

The lamellar grating spectrometer was used for the study of noise tubes and mercury lamps as schematically shown in Fig. 25. For the mercury lamps an f/1 mirror concentrates the light onto the entrance aperture of 1" diameter (not completely filled with the 100 watt lamp).

The noise tube with its antenna horn was placed directly at the 1" entrance aperture and adjusted for maximum throughput with respect to the two f/2 mirrors (8" diameter, f = 16") and the lamellar grating. Using the angle of the horn as a guide for the divergence of the radiation, the 8" mirror should just be completely filled when the apex of the horn was placed 16" away. At the exit aperture a dipstick detector[15] or two differently constructed He cooled bolometers[3] could be used. The dipstick detector was a He-cooled bolometer constructed in collaboration with L. Mosley of NASA Goddard Space Flight Center and similarly as described by Nishioka et. al.(ref. 18). The bolometer element was placed at the end of an evacuated light pipe in the center of a small hemisphere. A crystal quartz lens of 2-3mm thickness and 1mm black polyethylene were used as cooled filters for rejection of background radiation. The NEP of this detector was compared with detectors calibrated by Infrared Laboratory, Inc. and estimated to be 10^{-12}. The two bolometers from Infrared Laboratory were slightly different. Bolometer I uses an absorbing area of 3 x 3mm^2 and a straight concentration cone with a smaller opening of 3.5mm and had an NEP of 2.5×10^{-14}.

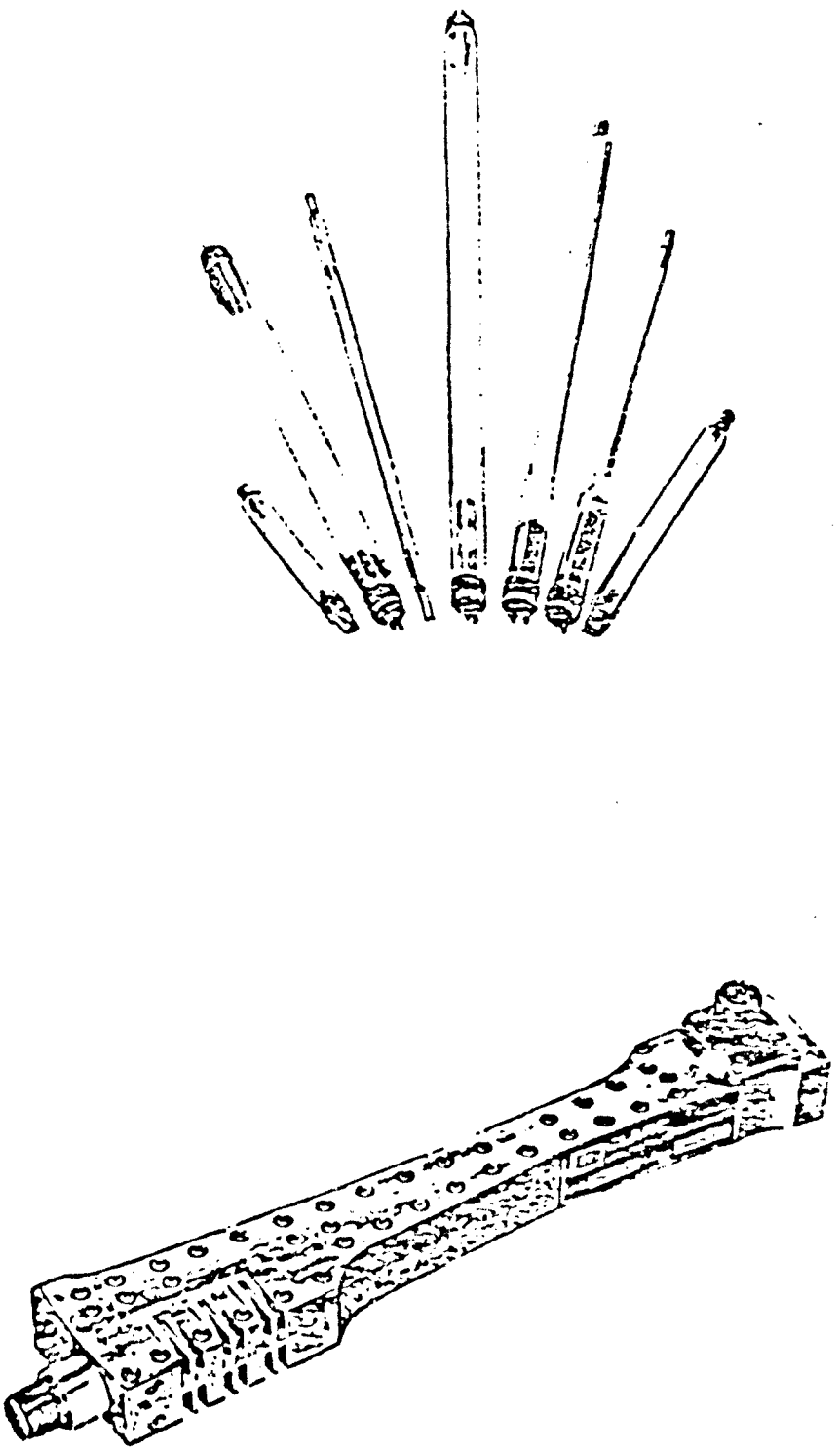

Figure 24. Noise tubes for the millimeter region.

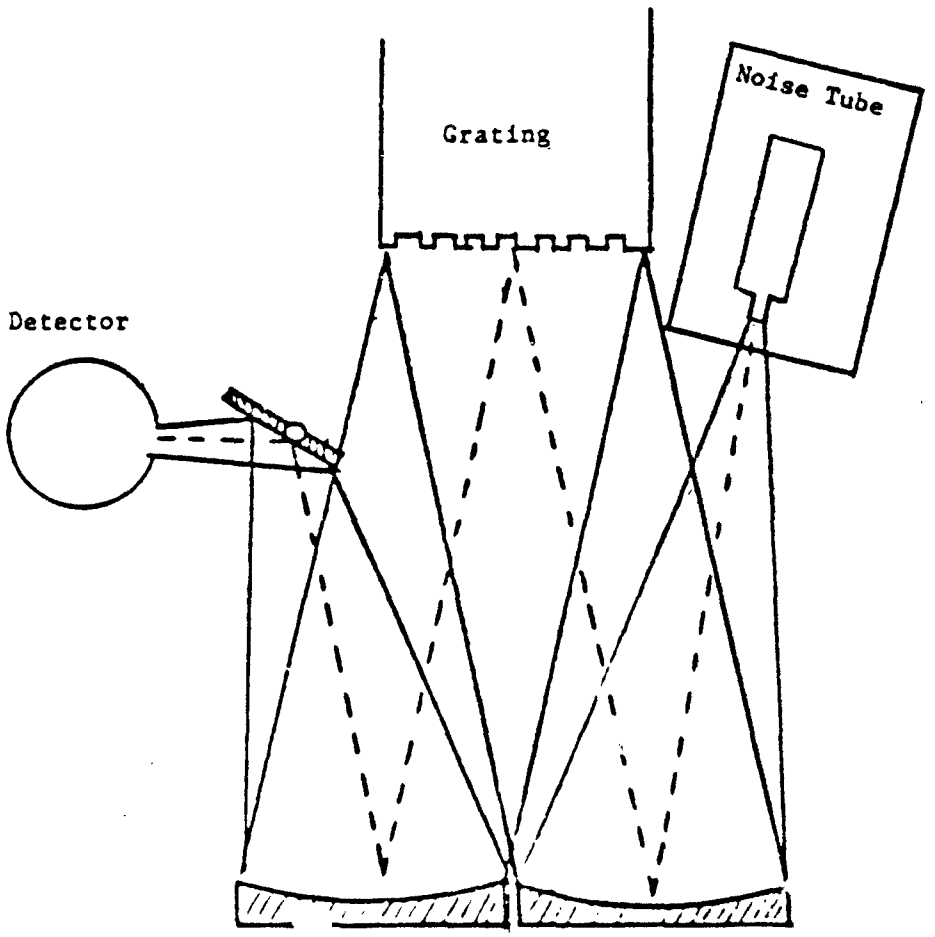

Figure 25. Lamellar grating used with noise tube as source.

Bolometer II uses a 4 x 4mm^2 area, a Winston cone with 5mm opening and had an NEP of 5.6 x 10^{-14}. The larger opening of the concentration cones for these two detectors was about 1/2" and the length of the two cones was about equal (4"), the light pipe connection to the teflon windows were, however, slightly different. For all three detectors, the incident light filled about an area of 1/2" and a solid angle corresponding to f/2 optics. Using the mercury lamp, an additional filter of 3mm thickness black polyethylene was used with the dip stick detector. For some spectra a Plexiglas filter of 1/8" or 1/4" was used[19].

For some of the experiments the noise tube was used with a plane concave diverging plastic lens of radius of curvature of 6 cm. Since this lens showed less radiation throughput, it was removed and the reported experiments were made by placing the noise tube with antenna in the instrument so that the scanning area was filled. The concentration optic of the instrument toward the detector was considered not of optimum, hampering the comparison of the emitted radiation between the two instruments. As detectors, one of the above mentioned He-cooled bolometers was used (with the straight cone). A third Infrared Lab. detector, Bolometer III, was a He cooled bolometer with an NEP of better than 10^{-13} but a concentration cone of smaller opening of 0.75mm diameter.

5.2 Results of Comparison

The results of comparison of the spectra obtained with a waveguide noise tube and a mercury lamp are limited by errors produced by the repeated alignment of the set-ups, the detector characteristics and the different optical systems including the concentration optics. The large number of different parameters to be observed for each comparison limits this discussion only to estimates.

5.2.1 Comparison of Power.

Using the lamellar grating set-up we have made power comparisons of the noise tube with a 100 watt a.c. mercury lamp. For shorter wavelengths than about 3mm the mercury lamp is more powerful than the noise tube.

Calling the ratio of the power of the mercury lamp to the noise tube M, we found that the ratio of M_1 (at $7.46cm^{-1}$) to M_2 (at $3.75cm^{-1}$) was 3. This ratio was the same for observations using the dip stick detector and the Bolometer II.

The noise tube without waveguide has been found considerably lower in its output compared to the mercury lamps in the far infrared. However, its lower content of near infrared and visible light reduces the filtering problem and offsets, for practical applications, the disadvantage of overall power output.

The reason that the noise tube without waveguide is less powerful may be explained by the smaller radiance. The area of generation of radiation for the same power input is spread over a much larger area.

5.3 Dependence of output power on wavelength and input current.

We have investigated with the dip stick detector the power output of the noise tube depending on the current. Fig. 26 and Fig. 27 show the spectra for 50mA and 125mA and a shift of output power to longer wavelength for operation with less current is clearly observed. This was confirmed using the Infrared Laboratory detectors (of higher sensitivity), see Fig. 28.

5.3.1 Source Noise

The spectra of the noise tube observed with the lamellar grating, dip stick detector and bolometers I and II show less noise. In the Nicolet spectrometer this difference was not apparent. We attribute it to the fact that with the Nicolet instrument we used a d.c. mercury lamp while with the lamellar grating an a.c. lamp was used.

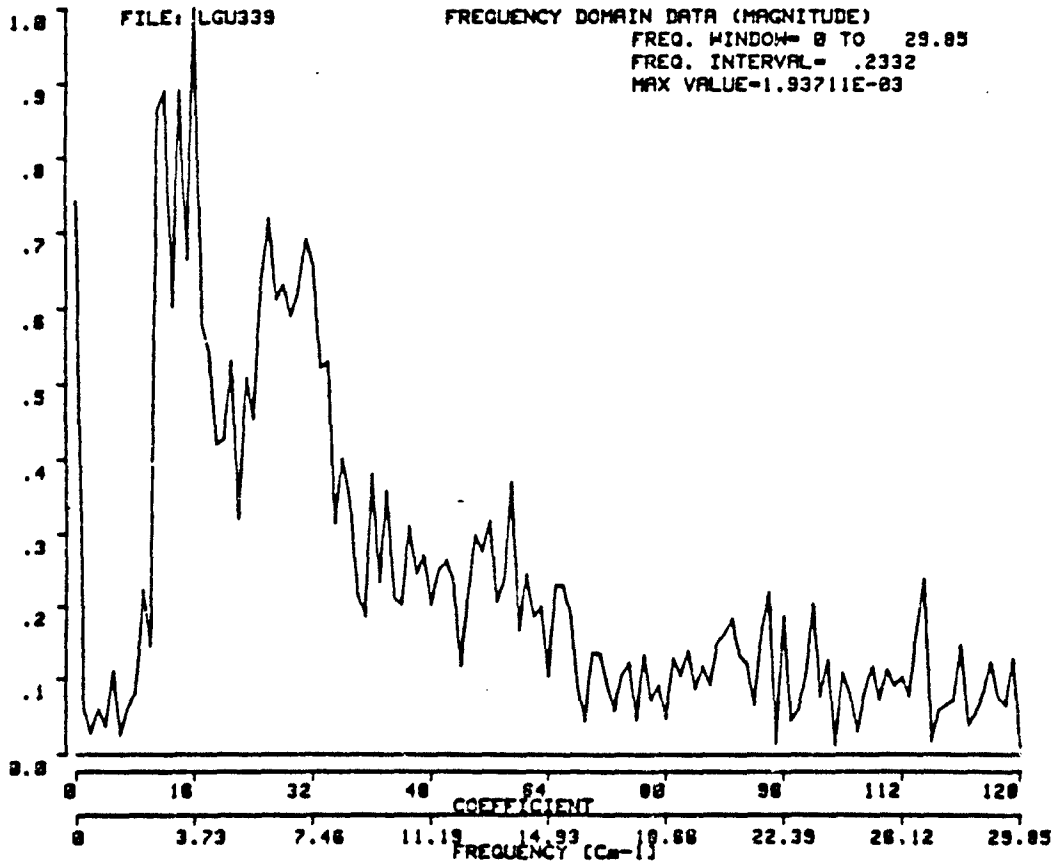

Figure 26. Spectrum of noise tube (50 mA current) obtained with dip stick bolometer and lamellar grating.

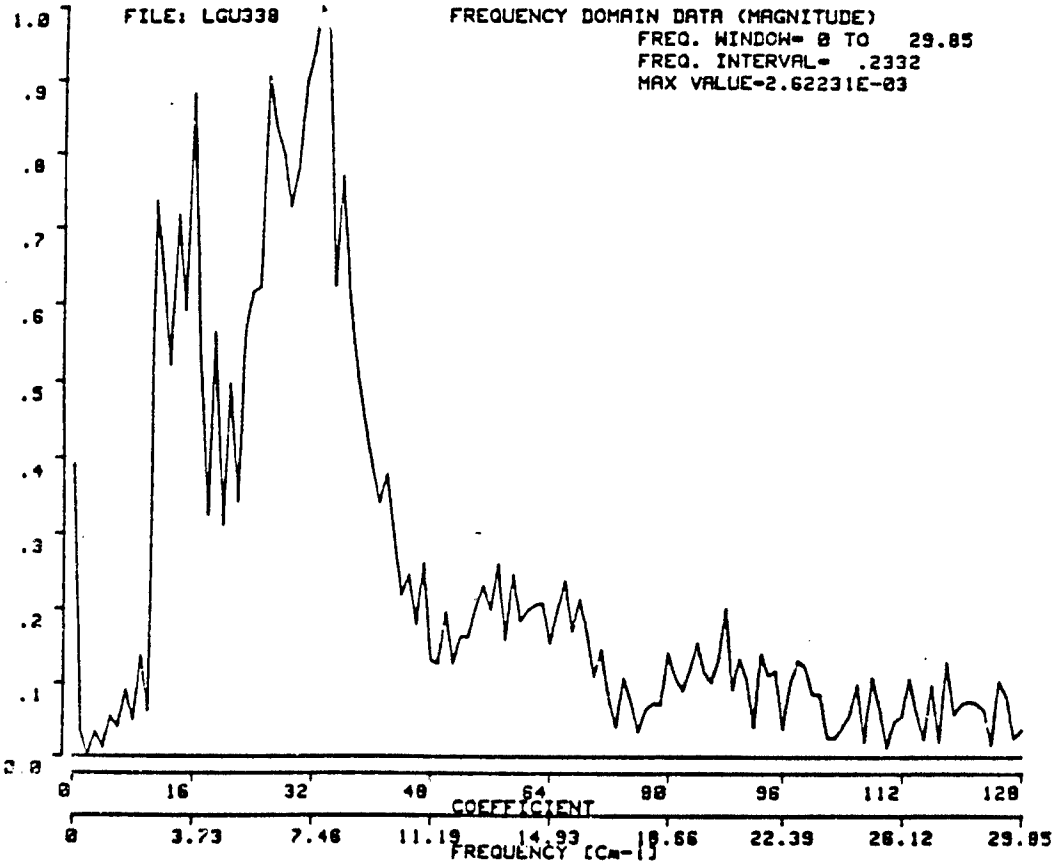

Figure 27. Spectrum of noise tube (125 mA current) obtained with dip stick bolometer and lamellar grating.

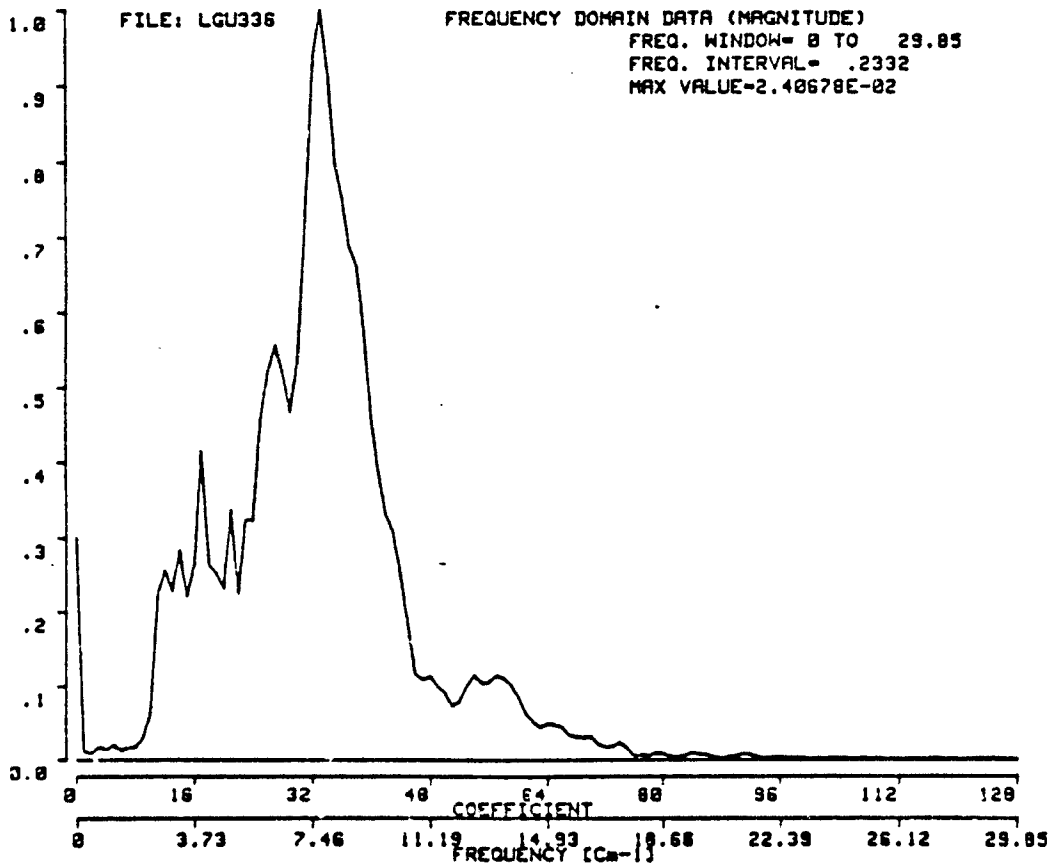

Figure 28. Noise tube output measured with lamellar grating and pumped He cooled bolometer II.

5.3.2 Long wavelength cut off.

All of our detectors regardless of the Noise Tube Power supply setting displayed a long wavelength cutoff for the noise tube emission at approximately 2.1cm^{-1}. This is clearly seen in Fig. 29 which shows the spectrum obtained with the Nicolet Spectrometer and Bolometer II. Using Bolometer III having a smaller hole of the concentration cone, one finds that a reduction of long wavelength transmission is observed, see Fig. 30.

All spectra taken using the C. P. Clair, N.T. displayed a very similar transmission pattern between 2cm^{-1} to approximately 10cm^{-1}. These spectra were very similar to the information obtained in a study on the frequency calibration of a Noise Tube[20]. The pattern appears almost exactly the same regardless of the detector or the spectrometer used. We therefore can conclude that this is the characteristic transmission spectrum for the Noise Tube manufactured by C. P. Clair.

5.4 Filtering.

It has been shown [ref.19] that Plexiglas is a superior far infrared filter and the cutoff frequency shifts to longer wavelengths as the thickness of the Plexiglas is increased. We see an interesting result with the Noise Tube. Not only does the cutoff frequency change but the transmission drops dramatically. We see a significant decrease in transmission using the 1/2 inch thick piece of Plexiglas and have observed a flat response when using a 3 inch thick piece of Plexiglas.

When using an ac mercury lamp along with a piece of 3 inch thick Plexiglas as a filter we obtained the spectrum shown. Fig. 8. According to Yon and Sievers[19] the cutoff frequency for a piece of 3 inch thick Plexiglas should be at approximately 8cm^{-1} which is true for the spectrum shown. The spectrum obtained in this fashion covers the region from 1.25cm^{-1} (8 mm) to 8cm^{-1} (1.2 mm). This clearly highlights almost the entire millimeter spectral region. Therefore the ac Mercury lamp is an excellent source for the millimeter wave spectral region.

6.0 Fourier Transform Spectrometer For The 1 To 10 mm Region.

6.1 Introduction

Fourier transform spectroscopy applied to the millimeter wavelength region may provide continuous spectra desirable for the study of material properties over several octaves of the spectrum. This method has been used in the submillimeter wavelength region using a Mercury lamp. In the mm-wave region the emission of the mercury lamp is so weak that only with very sensitive detectors spectra can be obtained.

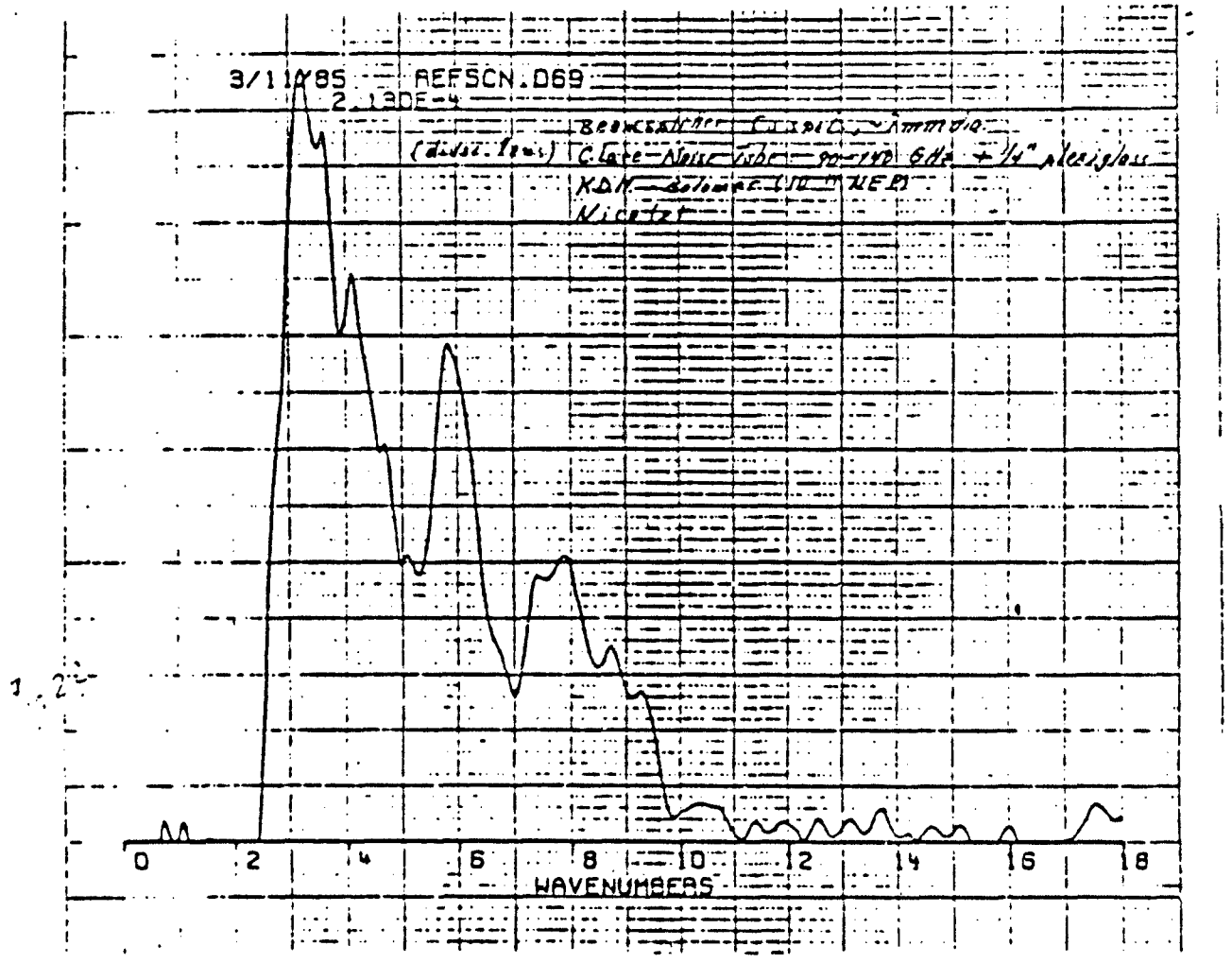

Figure 29. Spectrum of noise tube obtained with the Nicolet spectrometer and pumped He cooled bolometer II.

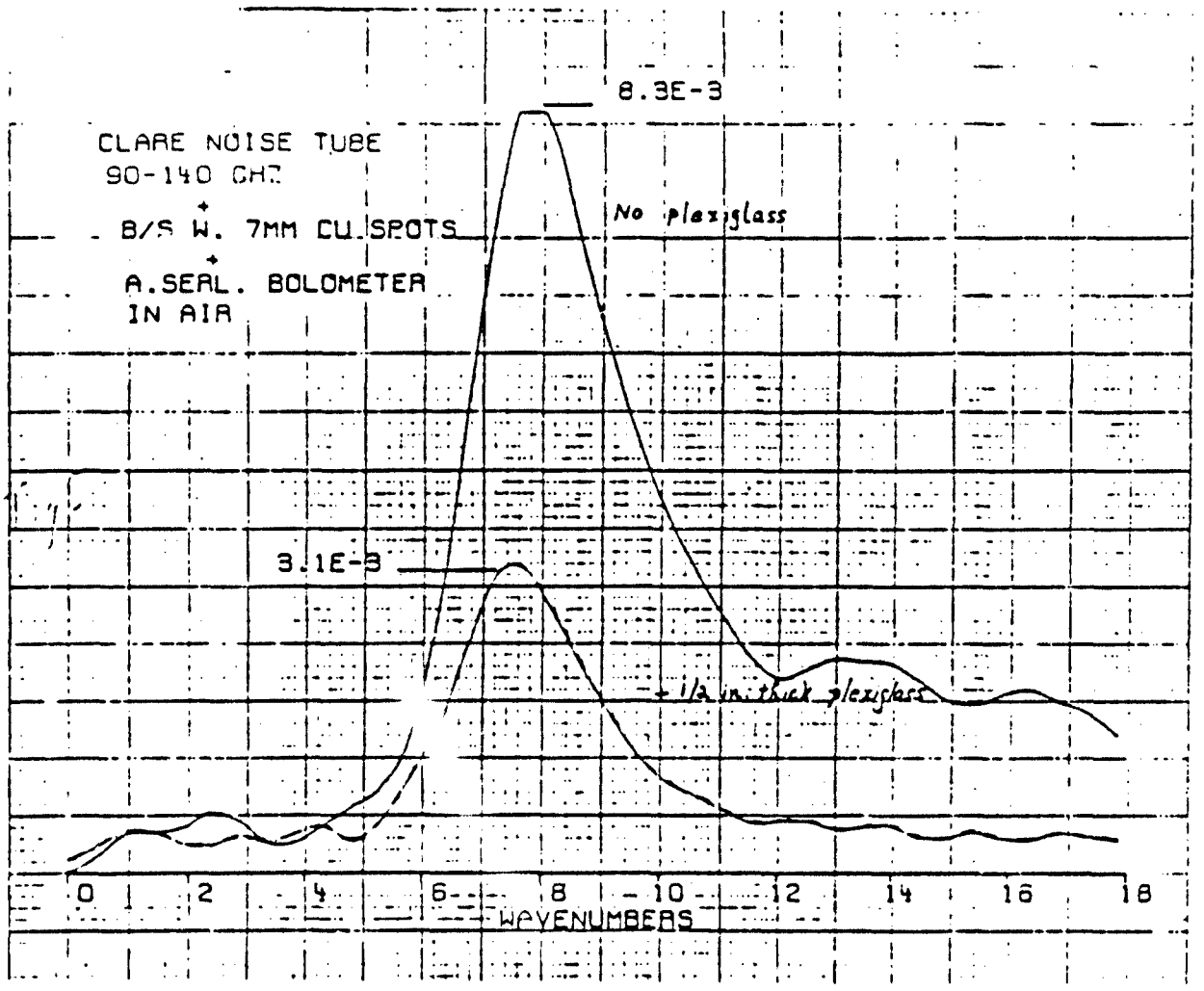

Figure 30. Noise tube emission measured with the Nicolet spectrometer and He cooled bolometer III.

We have used a lamellar grating because of its high efficiency and simplicity and a pumped He-cooled detector. The source was a 250 Watt ac Mercury lamp. Noise tubes have not been used since their spectral emission is more limited than a black body emitter.

The most important application of this spectrometer was the measurements on a cloud chamber filled with aerosols of powders. The air powder mixtures are only stable for about 5 minutes after generation. Therefore, it was requested that an interferogram could be taken within this time span. We have taken a 32 point interferogram in 2 min and 50 sec and obtained a useful spectrum.

6.1.1 Spectrometer

The spectrometer is shown in Fig. 31. The lamellar grating has a grating constant of 1.8 cm and the plates could be moved 7.5 cm from the zero position. The grating was used with the plates in horizontal position and the plates were made of aluminum. One stack of plates was fixed, the other was mounted on a carrier and could be moved with a stepping motor.

A 250 Watt ac Mercury lamp was used as the source and two 10" diameter spherical mirrors of focal length 16" were used as collimators and for concentration of the light onto the detector. The path length between the two spherical mirrors was 8 meters.

The detector was a pumped He-cooled bolometer manufactured by Infrared Laboratories, Inc. The absorbing element of the detector made of a thin diamond plate has a size of 4x4 mm and the NEP given by the manufacturer was 5.6×10^{-14}. The light was concentrated onto the detector element using a Winston cone with a smaller opening of 5.4 mm.

To obtain a single sided interferogram in 2 min and 50 sec we used a time constant of 1 sec and 32 points, taken step by step. The interferogram is shown in Fig. 32 and the transformed spectrum in Fig. 33. The strong features in the spectrum are interference fringes of the lamp or possibly some filters. The bolometer is equipped with filters having a long wavelength path at 30 cm^{-1}. In addition we have used a 3" thick plexiglas plate to pass the millimeter region[19].

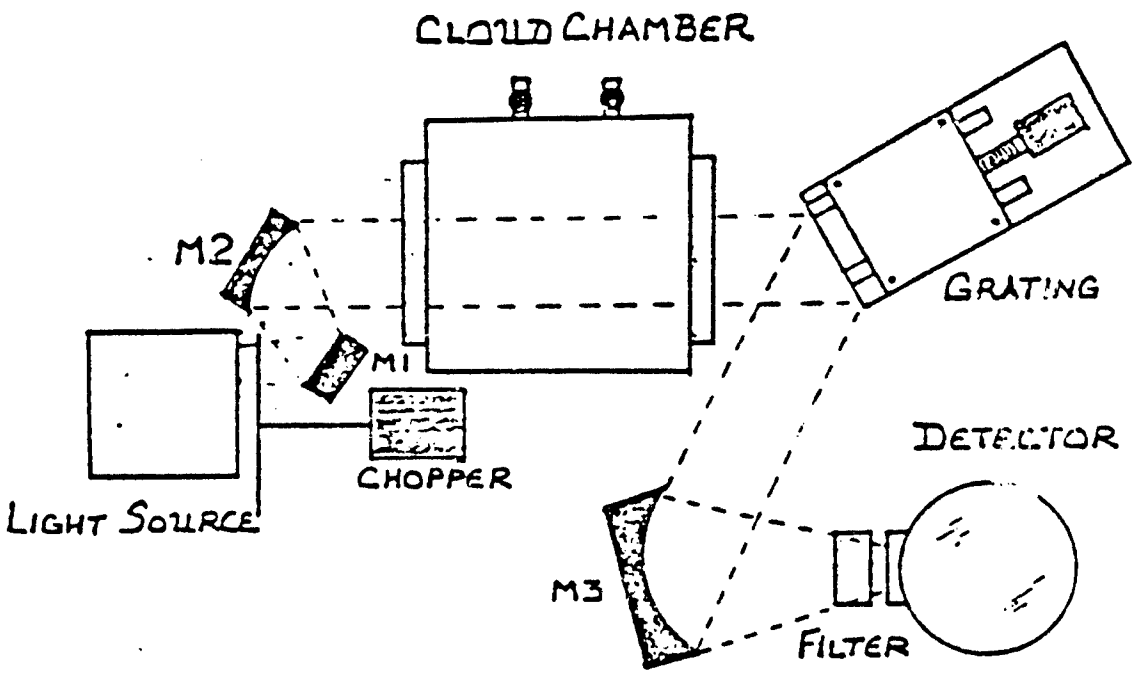

Figure 31. Spectrometer set-up using a cloud chamber or gas cell in atmospheric pressure environment.

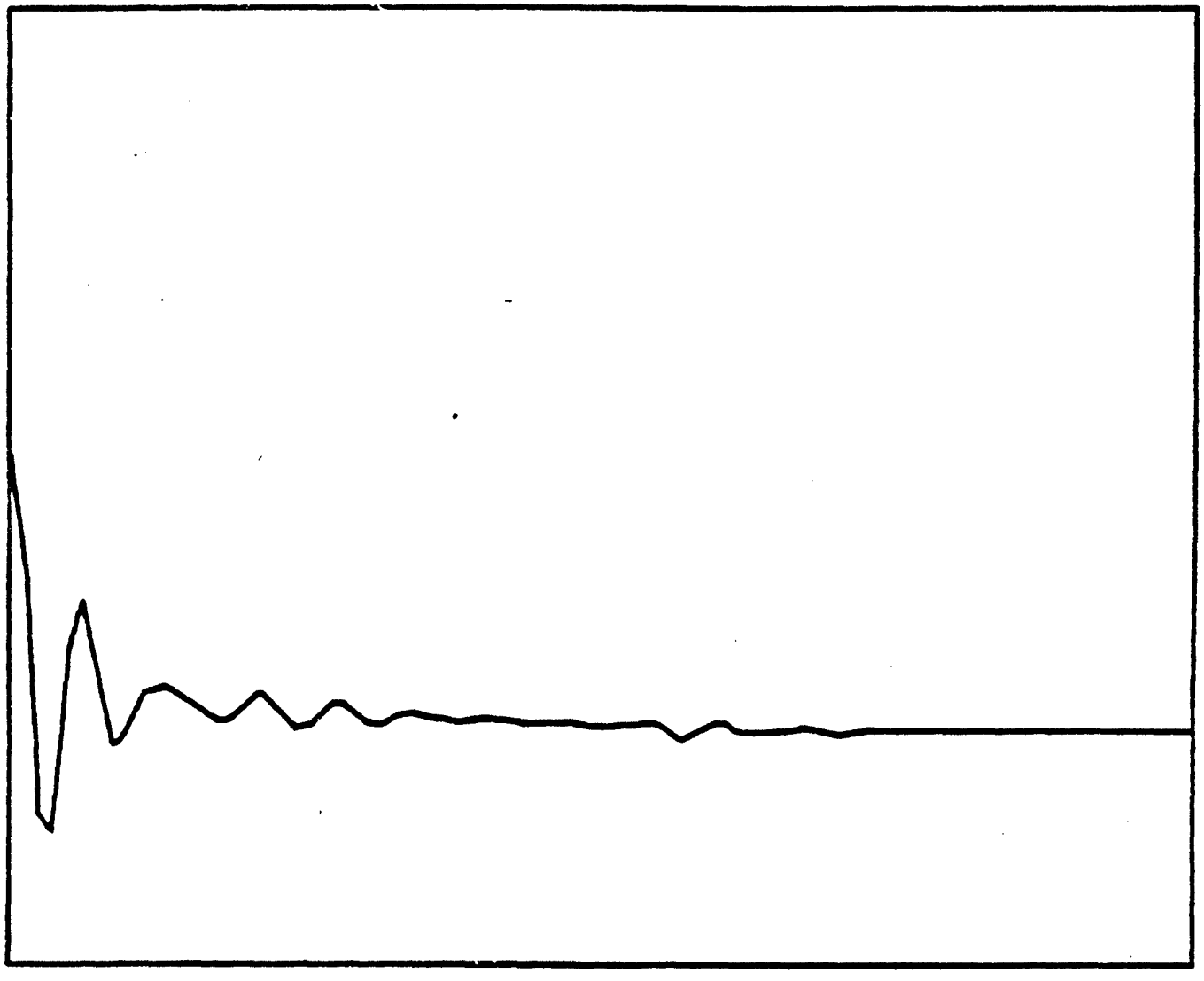

Figure 32. Single sided interferogram of 32 points, taken in 2 min. and 50 sec.

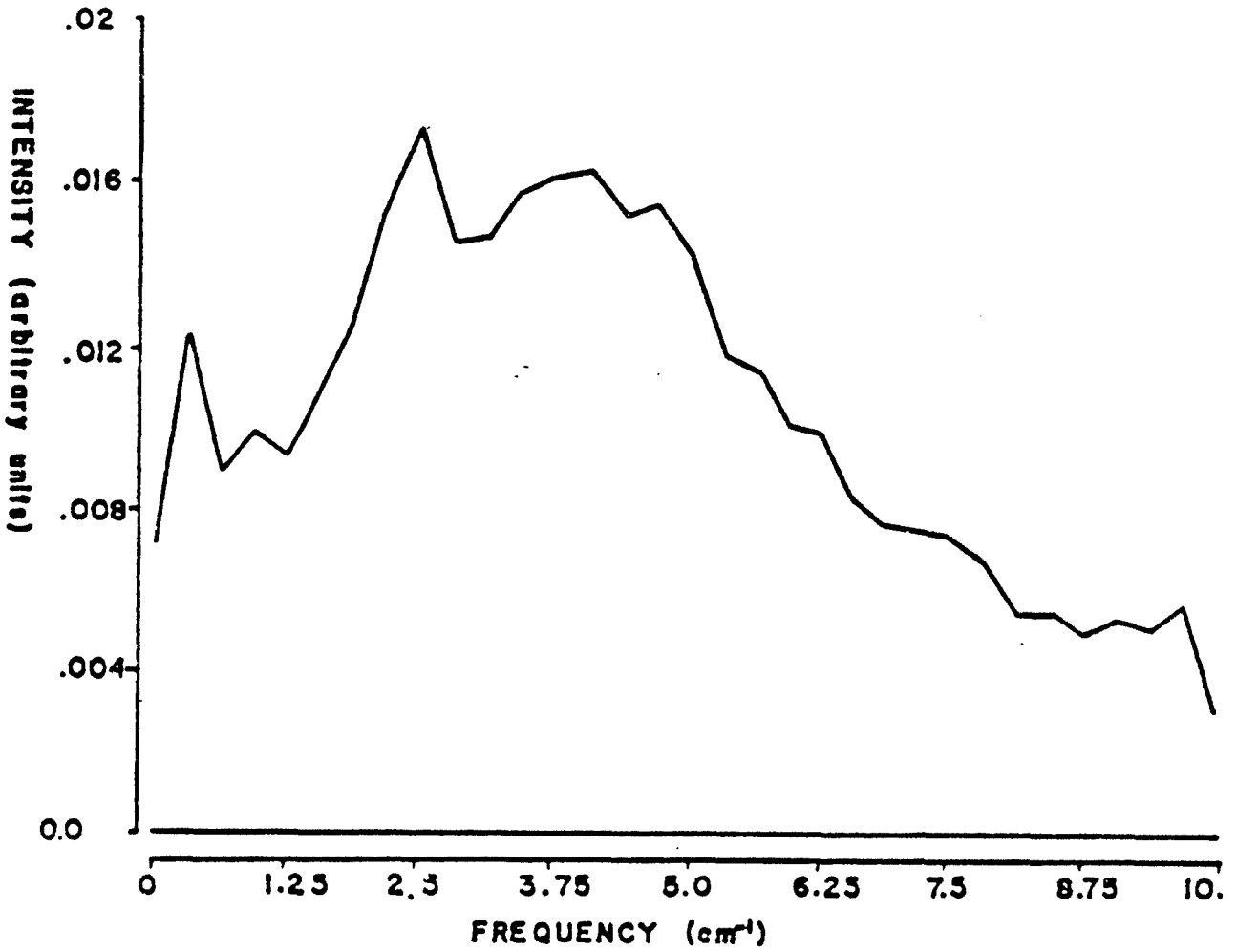

Figure 31 Spectrum of transformed interferogram of Fig. 2 in the 1 to 10 mm region.

6.1.1.1 Pure Rotation Spectrum of CH_3F

We have observed the pure rotation spectrum of methylflouride. A gas cell of 10" diameter and 30" length was used. The windows were made of 10 μm thick mylar and a certain amount of the gas was mixed with the atmosphere in the cell. Fig. 34 shows the observation of the lines with J=1,2,and 3 at wavelength 2.9mm, 1.95mm, and 1.46mm, respectively. The rotational constant was taken from the compilation of Townes and Schawlow[21], B=0.852 cm^{-1}. With this constant the population of the rotational states can be calculated, shcwing the intensity decrease as observed from J=3 to J=1, see Fig. 35.

6.1.2 Interference on metal dots of 1 mm diameter.

Some years ago we reported the use of beamsplitters for Michelson interferometers made from metal dots on thin mylar substrate[22]. These metal dots have diameters of 1 mm, a thickness of about 5000 A and were regularly arranged at an average distance of 1.7 mm. Since the arrangement of the dots on the mylar substrate is a capacitive grid, one expects a minimum at the wavelength equal to the lattice constant, this is shown in Fig. 36.

6.1.3 Observation on a cloud chamber

The lamellar grating spectrometer shown in Fig.1 was set up on a cloud chamber. The length between the two spherical mirrors could be changed between 1 and 8 meters without showing appreciable decrease in throughput, showing us that the millimeter wave radiation was well collimated by the optical spherical mirrors. The actual length of the cloud chamber light path was 2 m.

Transmission measurements were performed on in air dispersed graphite particles of 5 μm size (Asbury graphite). The powder was disseminated into the chamber at high pressure and an internal fan was used to keep the particles suspended. As the chamber filled, no visible light was observed passing the chamber. However, no attenuation of the millimeter wave region was observed, as shown in Fig. 37.

6.2 Absorption of thin Bi-films on dielectric fibers

We have evaporated thin Bi-films on dielectric meshes of average mesh size in the millimeter range, but not exactly periodic arranged. (Women's stockings) The reference samples without Bismuth showed no attenuation in transmission. Fig. 38 shows the relative transmission of layers of thickness of 100 A, 150 A and 200 A. Since we have used Bi-films of this thickness on sapphire plates for the construction of He-cooled Bolometers, we can conclude that the attenuation in Transmission measurements is mainly absorption and not reflection.

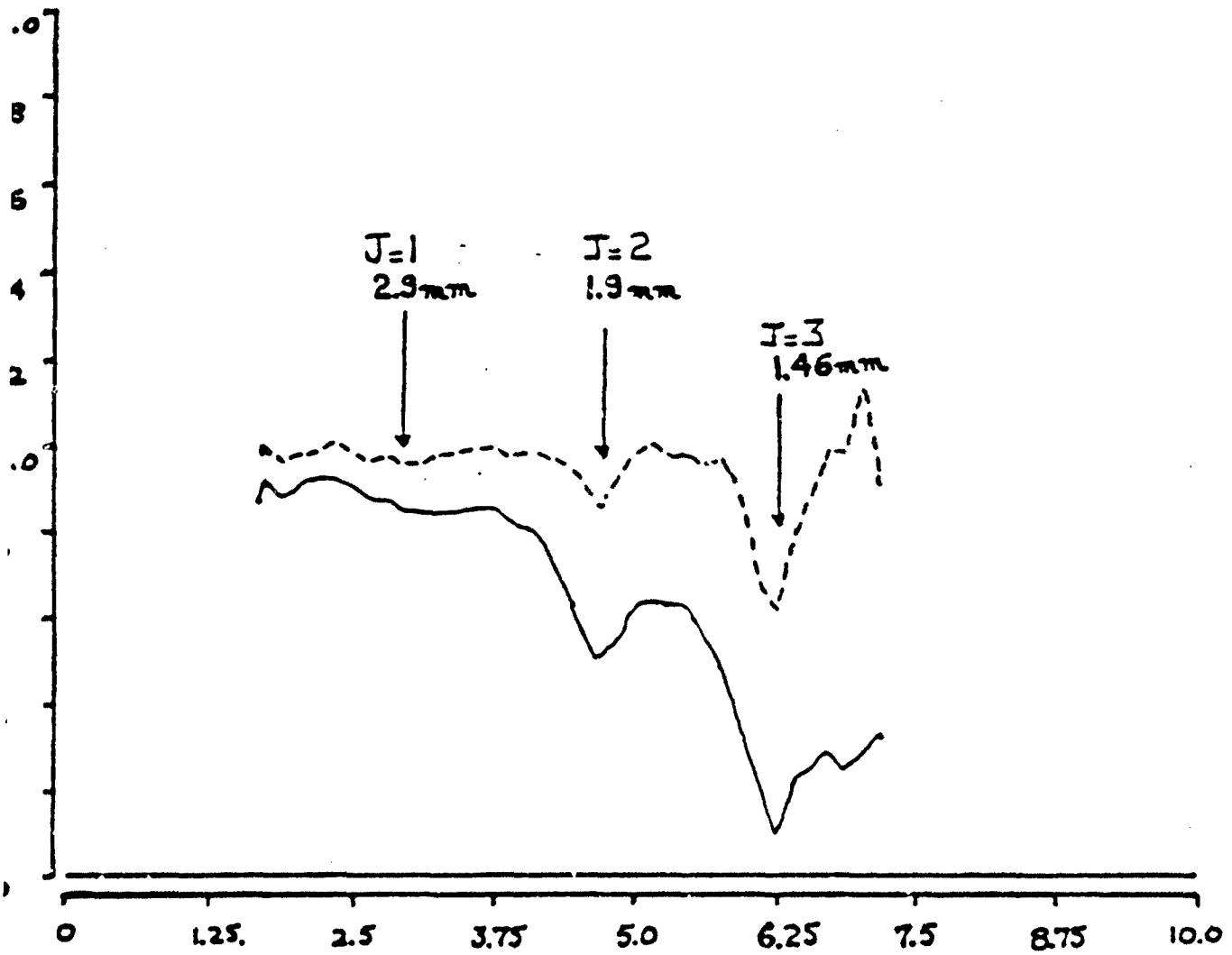

Figure 34. Ratioed Spectrum of CH_3F.

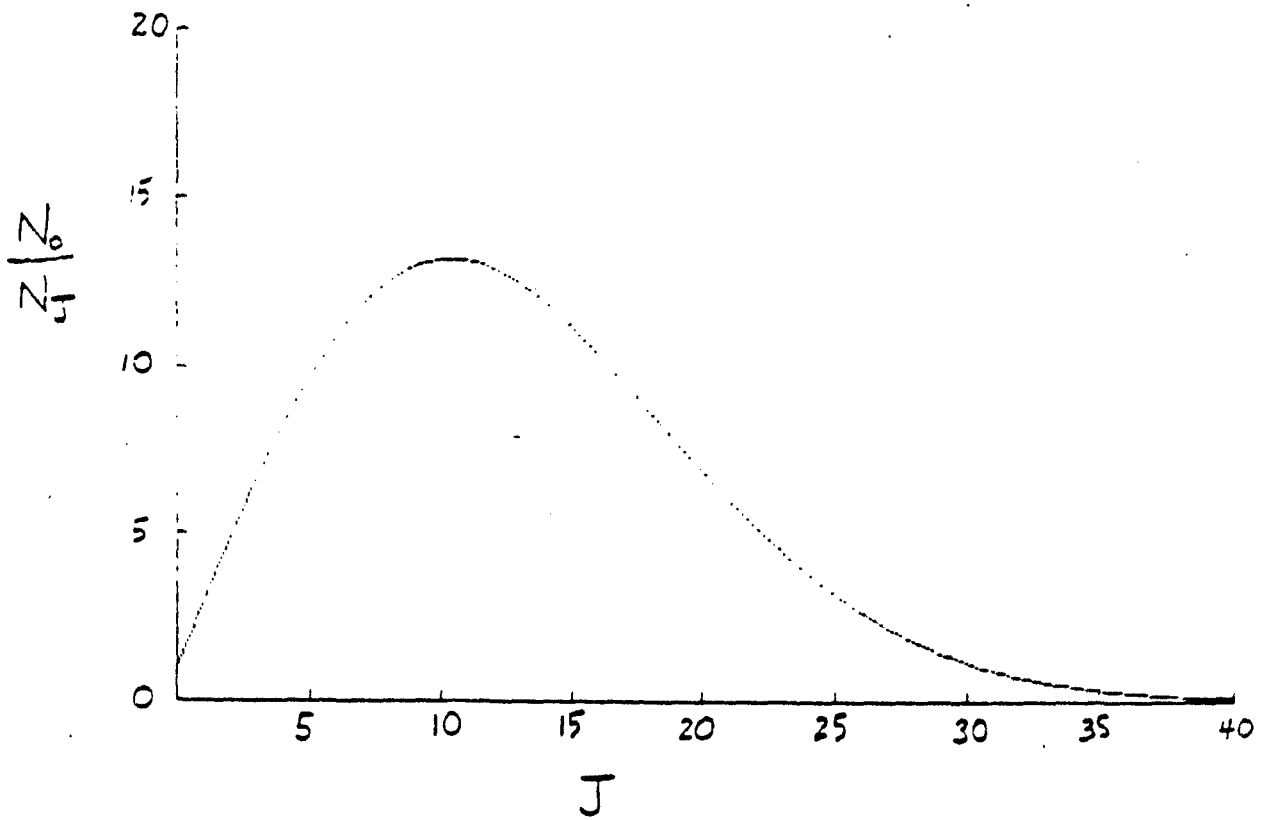

Figure 35. Population depending on J for CH_3F.

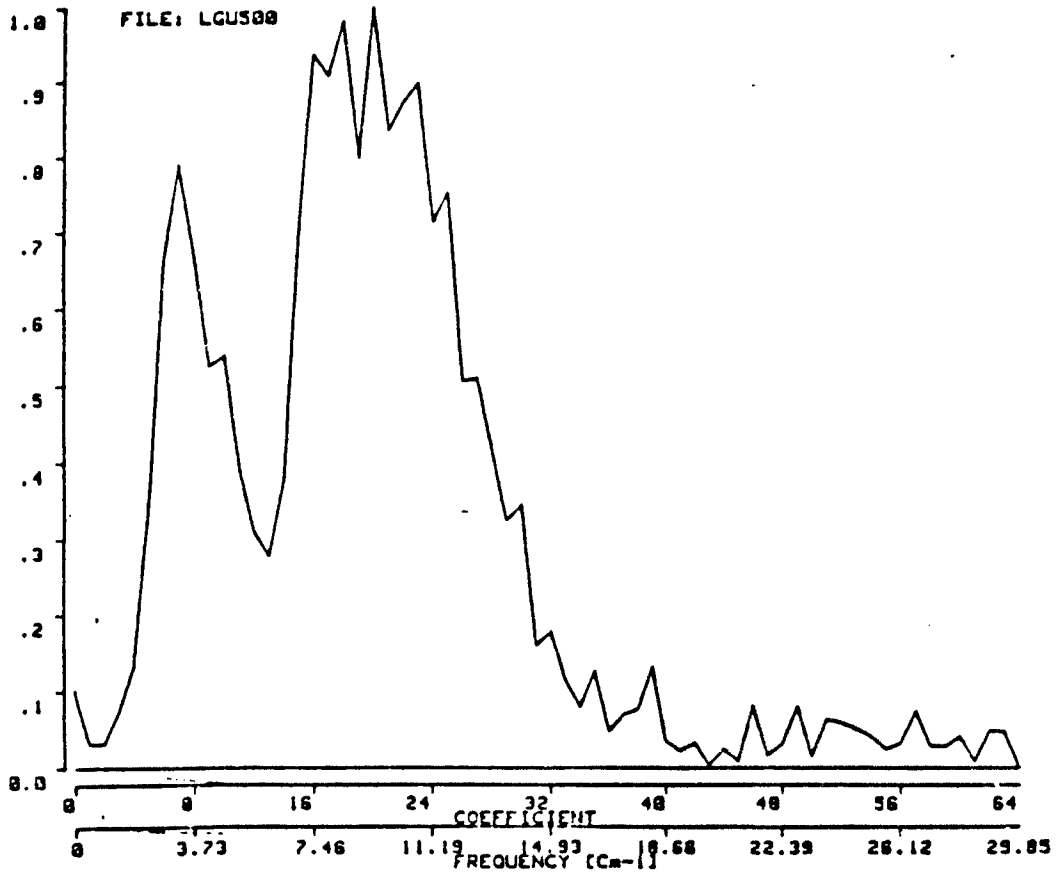

Figure 36. Transmission spectrum of Cu dots of diameter of 1mm on 10μm mylar substrate. The distance between the Cu dots is 1.7mm.

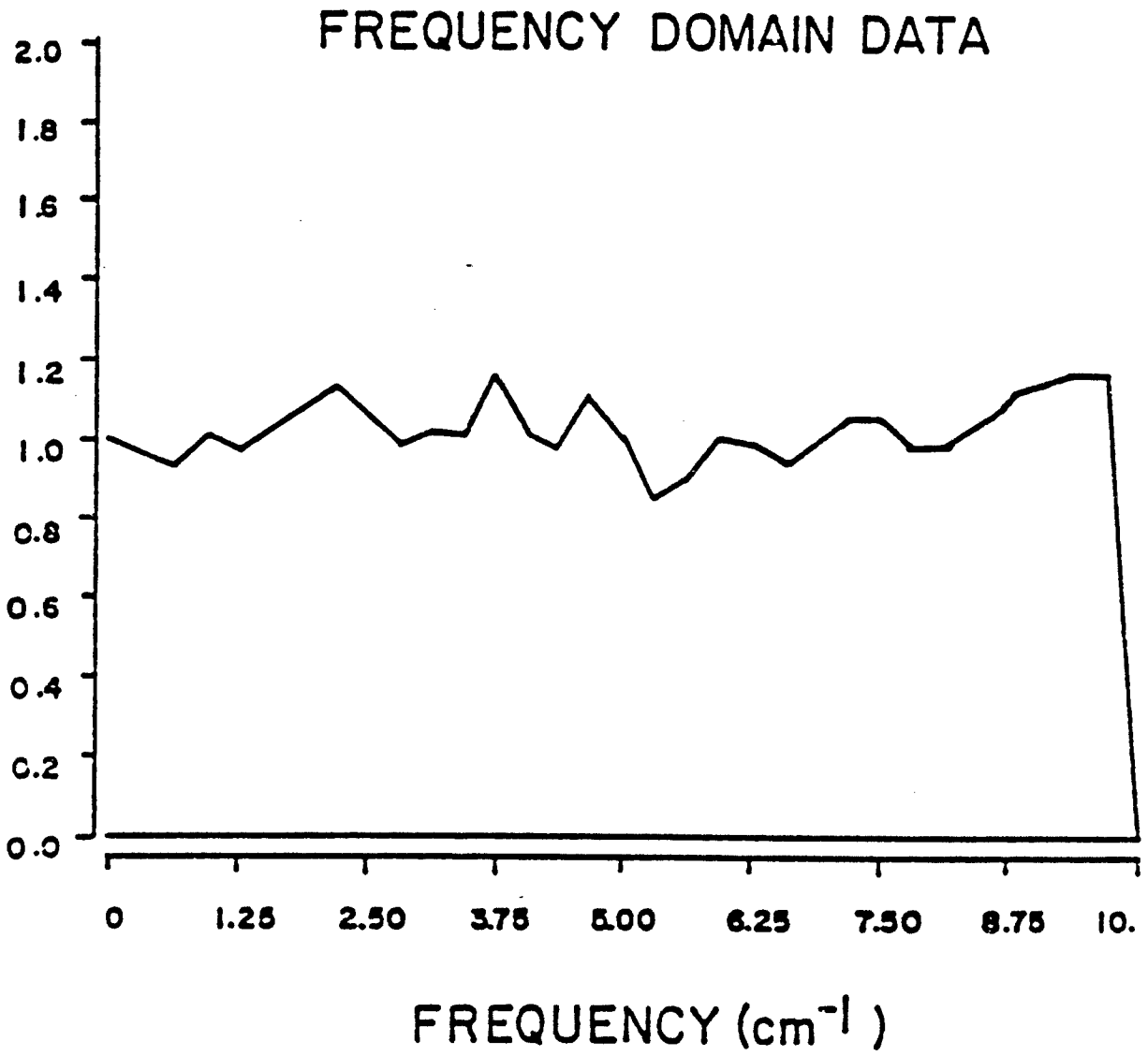

Figure 37. Ratioed spectrum of Asbury graphite (5um particle size) in a cloud chamber.

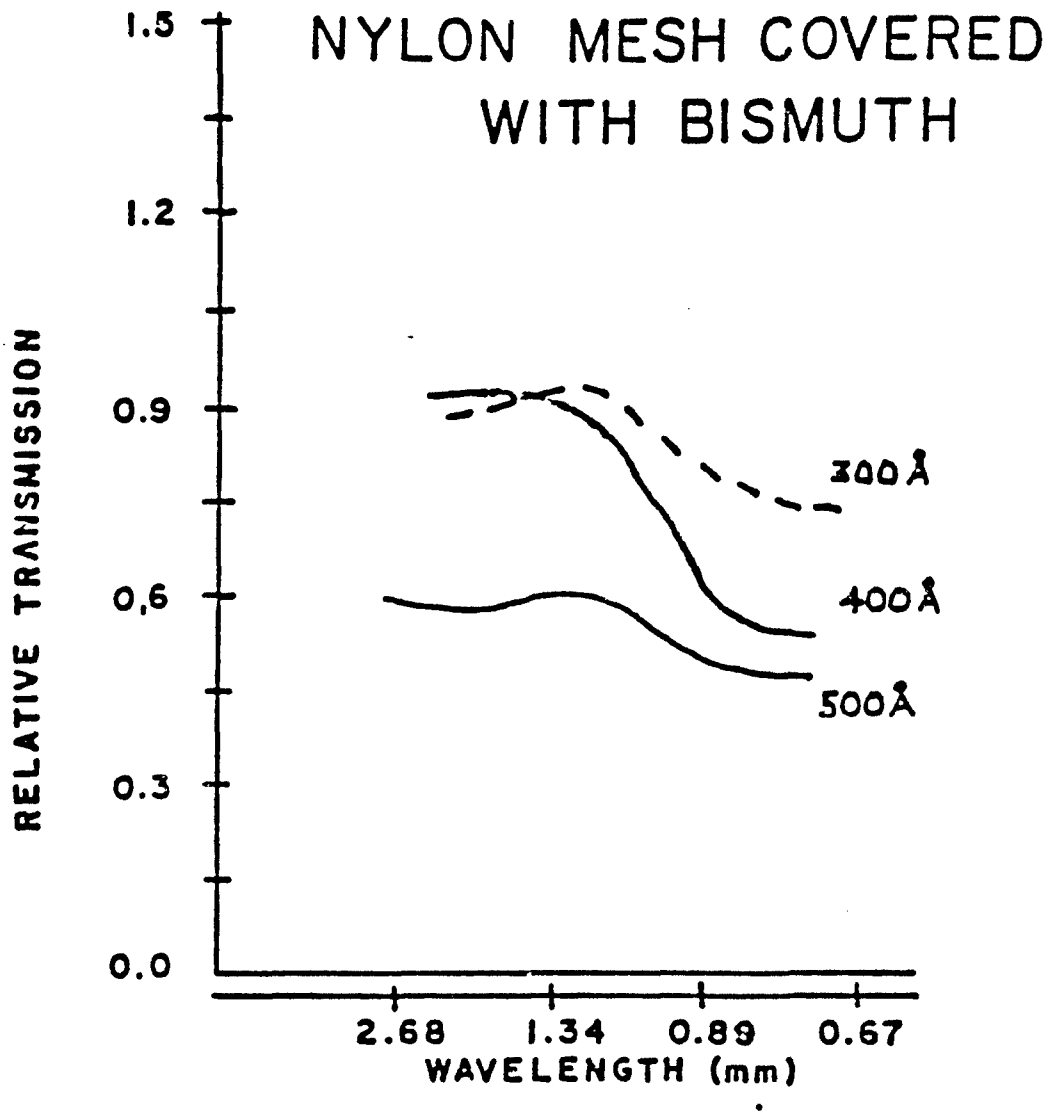

Figure 38. Absorption of dielectric mesh (nylon) covered with Bismuth.

References

1. J. Fahrenfort, Spectrochim. Acta 17, 698 (1961).1

2. V. P. Tomaselli, R. Rivera, D. C. Edewaard and K. D. Moller, Appl. Opt. 20, 3961 (1981).

3. B. Crawford, T. G. Goplen and D. Swanson, "The Measurement of Optical Constants in the Infrared by Attenuated Total Reflection," in Advances in Infrared and Raman Spectroscopy, Vol. 4, R. J. H. Clark and R. E. Hester, Eds. (Heyden, London, 1978), Chap. 2.

4. T. Hirschfeld, Appl. Spectrosc. 32, 160 (1978).

5. T. Hirschfeld, Appl. Spectrosc. 24, 277 (1970).

6. T. G. Goplen, D. G. Cameron and R. N. Jones, Appl. Spectrosc. 34, 657 (1980).

7. J. C. Maxwell Garnett, Philos. Trans. R. Soc. London Ser. A 203, 385 (1904); 205, 237 (1906).

8. Cabot Corp., Technical Report S-36, Boston, MA 02110.

9. E. M. Dannenberg, "Carbon Black," in Kirk-Othmer: Encyclopedia of Chemical Technology, Vol. 4 (Wiley, NY, 1978), pp. 631-666.

10. G. A. Niklasson and H. G. Craighead, Appl. Opt. 22, 1237 (1983).

11. S. G. Jennings, J. Opt. Soc. Am. 71, 923 (1981).

12. R. J. Bell, Introductory Fourier Transform Spectroscopy (Academic, NY 1972) Chap. 15.

13. K. D. Möller and V. P. Tomaselli, "Fourier Transform Spectroscopy," in Proceedings, 1982 Chemical Systems Laboratory Scientific Conference on Obscuration and Aerosol Research, R. H. Kohl, Ed. (Special Publications ARCSL-SP-83011, 1983), p. 145.

14. D. A. Naylor, R. T. Boreiko and T. A. Clark, "Mylar Beam-Splitter Efficiency in Far Infrared Interferometers: Angle of Incidence and Absorption Effects," Appl. Opt. 17, 1055 (1978).

15. J. Kachmarsky, C. Belorgeot, A. Pluchino and K. D. Möller, Far-infrared high-resolution Fourier transform spectrometer: applications to H_2O, NH_3, and NO_2 lines, Appl. Opt. 15, 708 (1976).

16. A. E. Costley, J. A. How and D. Vizard, Third International Conference on Submillimeter Waves and Their Applications, University of Surrey, England.

17. Infrared Laboratory Inc, 1808 East 17th St., Tucson, AZ 85719.

18. N. S. Nishioka, P. L. Richards and D. P. Woody, Appl. Opt. 17, 1562 (1978).

19. K. K. Mon and A. J. Sievers, Appl. Opt. 14, 1054 (1975).

20. C. P. Clair and Company, General Instrument Corporation, TD/TN April, 1979.

21. Microwave Spectroscopy, C. H. Townes and A. L. Schawlow, McGraw-Hill Book Company, Inc., NY 1955.

22. K. D. Möller, V. P. Tomaselli, J. Colosi and R. G. Zoeller, Appl. Opt. 23, 3075 (1984).